#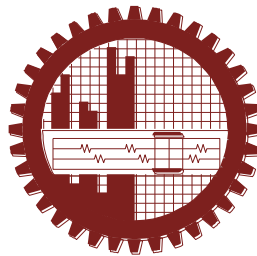 DIRECT CURRENT ELECTRICAL CONDUCTION MECHANISM AND OPTICAL PROPERTIES OF PLASMA POLYMERIZED O-METHOXYANILINE-N,N,3,5-TETRAMETHYLANILINE COMPOSITE THIN FILM

Md. Ahaduzzaman Deraz

Roll No. 0409143027F

Session: April, 2009

DEPARTMENT OF PHYSICS

BANGLADESH UNIVERSITY OF ENGINEERING AND TECHNOLOGY
Dhaka-1000

September, 2015

DIRECT CURRENT ELECTRICAL CONDUCTION MECHANISM AND OPTICAL PROPERTIES OF PLASMA POLYMERIZED O-METHOXYANILINE-N,N,3,5-TETRAMETHYLANILINE COMPOSITE THIN FILM
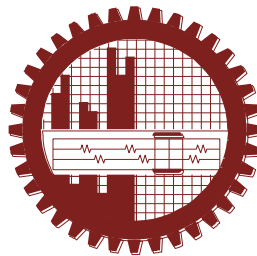
A dissertation submitted to the Department of Physics, Bangladesh University of Engineering & Technology in partial fulfillment of the requirement for the Degree of MASTER OF PHILOSOPHY (M.Phil.) IN PHYSICS

by

Md. Ahaduzzaman Deraz

Roll No. 0409143027F

Session: April, 2009

DEPARTMENT OF PHYSICS

BANGLADESH UNIVERSITY OF ENGINEERING AND TECHNOLOGY DHAKA-1000
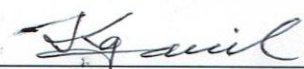
September, 2015

BANGLADESH UNIVERSITY OF ENGINEERING & TECHNOLOGY (BUET), DHAKA
**DEPARTMENT OF PHYSICS**

CERTIFICATION OF THESIS

The thesis titled **"DIRECT CURRENT ELECTRICAL CONDUCTION MECHANISM AND OPTICAL PROPERTIES OF PLASMA POLYMERIZED O-METHOXYANILINE-N,N,3,5-TETRAMETHYLANILINE COMPOSITE THIN FILM"** submitted by **MD. Ahaduzzaman Deraz**, Roll No-0409143027F, Registration No-0409143027, Session: April-2009, has been accepted as satisfactory in partial fulfillment of the requirement for the degree of **Master of Philosophy** (M. Phil.) in Physics on 29 **September, 2015.**

BOARD OF EXAMINERS

1. (_____)
   Dr. Md. Abu Hashan Bhuiyan
   Professor,
   Department of Physics, BUET, Dhaka

   Chairman
   (Supervisor)

2. (_____)
   Dr. Afia Begum
   Professor & Head
   Department of Physics, BUET, Dhaka

   Member
   (Ex-Officio)

3. (_____)
   Dr. Md. Forhad Mina
   Professor
   Department of Physics, BUET, Dhaka

   Member

4. (_____)
   Professor Dr. A T M Kaosar Jamil
   Department of Physics
   Dhaka University of Engineering And Technology (DUET),
   Gazipur

   Member
   (External)
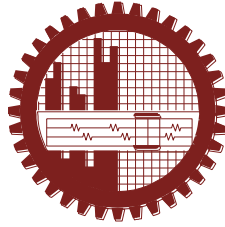
BUET

CANDIDATE'S DECLARATION

It is hereby declared that this thesis or any part of it has not been submitted elsewhere for the award of any degree or diploma.

_____

(**Md. Ahaduzzaman Deraz**)
Roll No. 0409143027 F
Session: April/2009

Dedicated to
My beloved Parents and Teachers
Who have inspired and influenced me in higher study

LIST OF FIGURES

LIST OF TABLES

Glossary

ABS	Absorbance
AC	Alternating Current
α	Absorption Coefficient
cc	Capacitively Coupled
d	Thickness
DC	Direct Current
DTA	Differential Thermal Analysis
DSC	Differential Scanning Calorimetry
E_{gd}	Direct transition energy gap
E_{gi}	Indirect transition energy gap
EDAX	Energy Dispersive Analysis of X-ray
FESEM	Field Emission Scanning Electron Microscope
F_L	Fermi Level
FTIR	Fourier Transform Infrared
I	Intensity of Radiation
IR	Infrared
J	Current Density
k	Boltzmann Constant
k	Extinction Co-efficient
PP(OMA-TMA)	Plasma Polymerized O-Methoxyaniline-N,N,3,5-Tetramethylaniline
PECVD	Plasma Enhanced Chemical Vapor Deposition
PVD	Physical Vapour Deposition
PF	Poole-Frenkel
rf	Radio Frequency
SCLC	Space Charge Limited Conduction
T_g	Glass Transition Temperature
T_m	Melting Point
TGA	Thermogravimetric Analysis
UV-Vis	Utraviolet-Visible
V	Voltage
ΔE	Activation Energy

λ	Wavelength
μ	Mobility of Charge Carrier
θ	Trapping Factor
σ	Electrical Conductivity
ε	Dielectric Constant
ε_0	Permittivity of Free Space

ACKNOWLEDGEMENTS

ABSTRACT

Plasma Polymerized O-Methoxyaniline-N,N,3,5-Tetramethylaniline (PP(OMA-TMA)) composite thin films of different thicknesses were prepared by a capacitively coupled glow discharge plasma reactor at room temperature. The composite liquid material was prepared by mixing equal volume ratio of Ortho-methoxyaniline and N,N,3,5-tetramethylaniline monomers. Under a suitable condition, the composite monomer vapor was produced and introduced into the reactor. During polymerization the power of the glow discharge was kept constant and deposition time was varied to get thin films of different thicknesses. The thickness of the plasma polymerized films deposited on chemically cleaned glass substrates was measured by using multiple-beam interferometric method. The differential thermal analysis (DTA) trace showed an exothermic increase up to about 575 K and then levels off where the TGA shows a decrease in weight (%) in 3 stages. Thus the thin films are observed to be stable up to about 575 K. The gradual fall of TGA may be a cause of thermal breakdown of PP(OMA-TMA) structure and expulsion of oxygen containing compounds.

The dependence of absorption coefficient (α) on the photon energy indicates that the absorption edge starts increasing around 2.25 eV and there is a rapid rise in α from 2.80 eV. The indirect and direct band gap of the PP(OMA-TMA) thin films in the range 2.13 to 2.80 eV and 3.13 to 3.73 eV respectively for samples of different thicknesses. As the thickness of the films increases electronic transition occurs from more depth of the samples which need more energy. It is found that the peak wavelength shifts to lower wavelength for thin films with higher thickness. It is observed in the current density - voltage (J-V) characteristics of PP(OMA-TMA) thin films that the current density increases nonlinearly with the applied voltage. It is found that the current density ohmic in the low voltage region and in the high voltage region the current density is nonohmic. The slope of the J-d plot ascertains in the higher voltage region that the type of charge conduction in PP(OMA-TMA) composite thin films is SCLC. Temperature dependence of J shows that there is hopping conduction in the lower temperature region and that is thermally activated in the higher temperature region.

CHAPTER I

GENERAL INTRODUCTION

1.1   Introduction

Preparation of materials and surface modification become the prominent area of research in the development of electronic and optoelectronic devices, sensors, etc. Plasma polymerization emerges as a most important technique for the preparation of organic thin films. By plasma polymerization organic vapours can be polymerized at around room temperature using plasma enhancement. It is stated that plasma polymeric materials have opened up a new area of synthesis, electronics, optoelectronics, microelectronics, biomedical and biosensors, etc. due to their sustainable structural, thermal, optical and electrical properties [1.1]. Plasma polymerized thin films have gained attraction among the researchers and scientist. Though radiation induced polymerization[1.2], conventional evaporation method [1.3], etc. can be used for the preparation of polymer thin films but plasma polymerization technique has advantages over these techniques, which can be used to deposit polymer thin films from almost any organic vapour [1.1]. The structures and properties of the plasma polymerized thin films are highly influenced by deposition power, electrode separation, monomer flow rate and steady state pressure in the reactor chamber. Plasma polymerized films are generally cross-linked and therefore insoluble in organic solvents. The chemical structure of the polymer is not exactly that of the monomer, largely due to abstraction of hydrogen atoms and/or fragmentation of monomers [1.4]. Studies of the structural, electronic, electrical and optical properties of organic polymers received immense interest for their potential in technology. Now-a-days there has been growing interest in the investigation of the optical and electrical properties of plasma polymerized organic thin composite films.

1.2   Review of Earlier Research Work

For the last several years because of attractive properties plasma polymerized thin films have investigated to find application in the field of microelectronics and photovoltaic [1.5]. It is necessary to synthesize high- performance polymer thin films by efficient physical techniques for advanced scientific and technological applications [1.4, 1.6, 1.7]. Plasma polymerized thin films may find applications in diodes, thin film transistors, switching elements, dielectrics, sensors, capacitors, optoelectronic devices, etc. [1.8, 1.9]. Shah Jalal et al. [1.10] prepared thin films of m-xylene by plasma polymerization method using a capacitively coupled reactor. They revealed from

polarized light microscopy and IR spectroscopic studies that films were smooth, pinhole free and structurally different from m-xylene.

At lower deposition powers, the polyterpenol films preserved more of the original monomer constituents, such as hydroxy functional groups; however, they were also softer and more hydrophilic compared to polymers fabricated at higher power [1.11]. Kamal and Bhuiyan [1.12] reported that the direct current conduction mechanism in plasma polymerized pyrrole−N,N,3,5-tetramethylaniline bilayer thin films was space charge limited conduction (SCLC). It has been shown by Chowdhury and Bhuiyan [1.13] that Poole-Frenkel (PF) mechanism was operative in the heat-treated plasma polymerized diphenyl films. In the radio-frequency (rf) and alternating current plasma polymerized aniline thin films it was found that the rf plasma polymerized thin films has a higher value of electrical conductivity compared to that of ac. Iodine doping enhanced the conductivity of this film considerably [1.14].

Majumder and Bhuiyan [1.15] employed electrical glow discharge technique for the preparation of plasma polymerized vinylene carbonate (PPVC) thin films of aluminum/thin film/aluminum sandwich structure at room temperature by a parallel plate capacitively coupled reactor. The structural investigation of the monomer VC and PPVC was performed by Fourier transform infrared spectroscopy. They found Ohmic current conduction in the low voltage region and non Ohmic conduction in the high voltage region and the most probable conduction mechanism in the PPVC thin films is of Schottky type.

Akther and Bhuiyan [1.16] investigated PPTMA thin films deposited at room temperature by a parallel plate capacitively coupled glow discharge reactor. IR investigation reveals that chemical structure of TMA retains to some extent in the PPTMA thin films. The current density-voltage (J-V) characteristics of PPTMA thin films of different thicknesses have been investigated at different temperatures. The J-V characteristics of PPTMA thin films with Al electrodes show ohmic behavior at the lower applied voltage region and SCLC dominated by exponential trap distribution at the higher voltage region. Arrhenius plots of J vs 1/T for the applied voltages 2 and 10 V, in the lower and higher temperature regions activation energies (ΔE) are estimated to be about 0.19 ± 0.02 and 0.85 ± 0.05 eV respectively.

Plasma polymerized perylene thin films prepared by Blaszczyk-Lezak et al. [1.17] and studied their optical properties. They noticed that films are highly absorbent, fluorescent and very flat with a root mean square (rms) roughness in the range 0.3-0.4 nm. This film can be used as decorating coatings due to high light absorbing power even the film is very thin. The optical and microstructural characteristics of this type of thin films make them suitable for their integration into photonic components for various nanometric applications.

Kipnusu et al. [1.18] investigated charge transport mechanism in thin Nandi flame cuticle biomaterial J-V characteristics showed ohmic conduction at low fields and SCLC at high fields. Phonon assisted variable range hopping (VRH) transport mechanism is dominant that takes place between two localized states in the temperature range of 330-440 K.

Olshausen et al. [1.19] observed alternation current (AC) loss and DC conduction mechanisms in polyethylene under high electric fields and reported that for the AC field the origin of charge carriers involved in hopping conduction process was found to be donor like states in the bulk of the insulator.

Ltaief et al. [1.20] investigated the dark and illuminated J-V characteristics of poly(2-methoxy-5-(2'-ethylhexyloxy)1-4-phenylenevinylene)   (MEHPPV)/   single-walled carbon nanotubes (SWNTs) composite photovoltaic cells. Using an exponential band tail model, the conduction mechanism has been analyzed for polymer only devices and composite devices, in terms of SCLC conduction mechanism. The relatively high values of series and shunt resistances was explained by a reduced photogeneration rate and increased recombination rate, which is exacerbated by the proportional metallic nanotubes in the composite layers.

Shah Jalal et al. [1.10] investigated the conduction mechanism in PPm-X thin films deposited using a capacitive coupled glow discharge reactor. J-V characteristics of the PPm-X thin films were investigated at different temperatures and different thicknesses. Nonlinear I-V characteristics were analyzed following three different mechanisms of carrier conduction. The conclusion is drawn in the way that the PF type of conduction is most probable in PPm-X thin films.

Afroze and Bhuiyan [1.21] investigated the electrical conduction mechanism in plasma polymerized 2-(diethylamino)ethyl methacrylate (PPDEAEMA) thin films deposited using a capacitive coupled glow discharge reactor. J-V characteristics for PPDEAEMA thin films studies different thickness and different temperature range from 298 to 423 K. J-V curves reveal that in the low-voltage region, the conduction current obeys Ohm's law and SCLC in the high-voltage region. The activation energies were estimated to be about 0.005-0.016 eV for 2 and 30 V of PPDEAEMA thin films of different thicknesses. The low-activation energies indicate that the thermally activated hopping conduction is operative in PPDEAEMA thin films.

Change in optical properties of as-deposited plasma polymerized 2, 6-diethylaniline (PPDEA) thin films due to iodine doping investigated by Matin and Bhuiyan [1.22]. PPDEA thin films of different thicknesses are synthesized by a glow discharge plasma polymerization method. The iodine doped PPDEA is found thermally stable up to about 560 K which is a bit lower as observed for as-deposited PPDEA. Increasing doping period it was found the direct and indirect optical transition energy gaps are decreased from 3.56 to 2.79 eV and 2.23 to 1.97 eV, respectively.

Plasma polymerized 1, 1, 3, 3-tetramethoxy-propane (PPTMP) thin films of different thicknesses were prepared by Afroze and Bhuiyan [1.23] through glow discharge using a capacitively coupled reactor. They found smooth, uniform and pinhole free films with aliphatic conjugation of C=C and C=O bonds. There was formation of C-O-C bond owing to rearrangement of oxygen due to heat treatment of PPTMP thin films. The allowed direct transition (E_{gd}) and indirect transition (E_{gi}) energy gaps were found to be about 2.92 to 3.16 eV and 0.80 to 1.53 eV, respectively, for as deposited PPTMP of different thicknesses. The E_{gi} of two different thicknesses heat treated at 673 K for 1 hour is 0.55 and 0.65 eV.

The structural analyses of PPTMA thin films have revealed that PPTMA thin films are formed with certain amount of conjugation, which modifies on heat treatment [1.24, 1.25]. From the UV-VIS absorption spectra, they found that the allowed direct and indirect transition energy gaps are modified when the samples are heat treated and Tauc parameter B for all the samples indicate an increase in structural order/conjugation in PPTMA thin films improved by heat treatment. Indirect energy gap varies from 1.49 to

1.86 eV with film thickness. J-V characteristics indicate that the conduction mechanism in PPTMA thin films is SCLC. From the electrical and optical measurements they suggest that the top of valence band and the bottom of the conduction band may have gap states and the middle of the energy gap may be equal to the high temperature activation energy.

Rahman and Bhuiyan [1.26] investigated plasma polymerized o-methoxyaniline (PPOMA) thin films of different thicknesses prepared using a parallel plate capacitively coupled glow discharge reactor. FTIR spectra reveal a decrease of absorption intensity and disappearance of some absorption peaks for PPOMA as compared to those of OMA, indicating the formation of the thin film with modified chemical structure. The E_{gd} and E_{gi} were found to be about 1.68 to 2.08 eV and 2.90 to 3.08 eV, respectively, for as deposited PPOMA of different thicknesses at room temperature.

Plasma polymerized pyrrole−N,N,3,5-tetramethylaniline (PPPy-PPTMA) bilayer thin films were prepared by Kamal and Bhuiyan [1.27] in using a capacitively coupled reactor. They reported that the E_{gd} and E_{gi} of PPPy-PPTMA bilayer thin films have been increased compared with the PPPy and PPTMA thin films.

Sajeev and Anantharaman [1.28] studied the carrier transport mechanism of polyaniline thin films prepared by rf plasma polymerization. It is found that the mechanism of carrier transport in these thin films is SCLC.

From the above review of literature, it can be seen that the investigation of optical and electrical properties of organic thin films are necessary to find suitable application. So the study of the DC electrical conduction mechanism and optical properties of plasma polymerized o-methoxyaniline-N,N,3,5-tetramethylaniline PP(OMA-TMA) composite thin film is undertaken for its application in devices.

1.3   Objectives of the Present Study

The aim of the present research is to prepare and to investigate the different properties of the Plasma Polymerized O-Methoxyaniline-N,N,3,5-Tetramethylaniline PP(OMA-TMA) composite thin films. The PP(OMA-TMA) composite thin films would be deposited at different deposition time, different power etc. to find the optimum condition for good sample deposition. In the present investigation, PP(OMA-TMA) composite thin films are prepared at optimized conditions by a capacitive coupled glow

discharge plasma polymerization method. The chemical structure and physical absorption co-efficient, optical energy gaps and dc electrical conduction processes properties of the eposited thin films would be investigated by the following ways.

Structural Investigations

- To investigate the chemical structure of the PP(OMA-TMA) thin films by Fourier transform infrared spectroscopy (FTIR).

- To investigate the structural degeneration by thermal analysis.

Optical Measurements

To study optical properties using UV-visible spectroscopy and to determine the absorption co-efficient, direct and indirect transition band gaps of the thin films.

DC Electrical Measurements

To perform dc electrical measurements performed at different temperatures on samples of different thicknesses to understand the DC conduction mechanism in PP(OMA-TMA) thin films. Thickness dependence of these parameters would be observed and analyzed.

The obtained results would be analyzed using existing theories to understand the structural, optical and DC electrical behavior of the thin films and also to understand their relations which may indicate some suitable applications of this type of material in the electrical, electronic and optical devices.

1.4   Structure of the Thesis

The format of the thesis is as follows:

Chapter I: This chapter basically focuses on the reviews of earlier research work of different plasma polymerized thin films and discusses the aim of this thesis work both from the academic and practical viewpoints.

Chapter II: The general aspects of polymers, plasma, plasma polymers, advantages and disadvantages of plasma polymers, different plasma polymerization techniques are discussed in this chapter. And this chapter also presented the application of plasma polymerized organic thin films and theories of different measurements.

Chapter III: This chapter discusses materials and experimental details such as plasma polymerization set up, generation of glow discharge, film thickness measurements, sample formation etc. related to the thermal, structural, optical and DC electrical characterizations of PP(OMA-TMA) composite thin films.

Chapter IV: This chapter includes the results and discussion of the structural, thermal, optical and DC electrical observations.

Chapter V: This chapter is arranged with conclusions of the present work and suggestions for future research on those materials.

References

[1.1]   d'Agostino, R., "Plasma Deposition, Treatment and Etching of Polymers", Academic Press, San Diego, CA (1990)

[1.2]   Stuart, M., "Dielectric properties of cross-linked polystyrene film formed in the glow discharge", *Nature* 199, 59-60, 1963.

[1.3]   White, M., "Vacuum Evaporation of Polythene", Vacuum, 15, 449-450, (1965)

[1.4]   Ming-Zhu Wang, Shu-boFeng, Xiong-Yan Zhan, "Preparation of plasma poly(1-isoquinolinecarbonitrile) thin film," J. Mater. Sci, 41, 3609-3615, (2006).

[1.5]   Polonskyi, O., Matousek, J., Drabik, M., Kousal, J., Choukourov, A., Slavinska, D., Biederman, H., Pleticha, D. and Hanley, L., "Deposition and basic properties of thiophene plasma polymer films", WDS'08 Proceedings of Contributed Papers, **Part III,** 159–162, (2008).

[1.6]   Morosoff N., D'Agostino R. (Ed), "In Plasma deposition, Treatment and Etching of Polymers", Academic Press, San Diego, CA, (1990).

[1.7]   Inagaki N, "Plasma Surface Modification and Plasma Polymerization", Technomic Publishing Co. Inc., New York, (1996).

[1.8]   D'Agostino, R, (Ed.), "Plasma Deposition, Treatment and Etching of Polymers" Academic Press, Boston, (1990).

[1.9]   El-Nahass, M. M, Abd –El- Rahman, K. F., Darwish, A. A. A , "Electrical conductivity of 4-trycyanovinyl-N,N-diethylaniline", Physica B, 403, 219-223, (2008).

[1.10] Shah Jalal A.B.M., Ahmed, S., Bhuiyan A.H., and Ibrahim, M., "On the conduction mechanism in plasma polymerized m-xyle thin films". Thin Solid Films, 295, 125-130. 1997.

[1.11] Bazaka, K., Jacob, M. V., and Bowden, B. F., "Optical and chemical properties of polyterpenol thin films deposited via plasma-enhanced chemical vapor deposition", J. Mater. Res., 26 (8), 1018-1025 (2011), DIO: 10.1557/jmr.2011.23

[1.12] Kamal M. M., and Bhuiyan, A. H., "Direct current electrical characterization of plasma polymerized pyrrole-N,N,3,5 tetramethylaniline bilayer thin films", J. Appl. Polym. Sci. Vol. 125, 1033–1040, (2012).

[1.13]   Chowdhury F-U-Z., Islam A.B.M.O., and Bhuiyan A.H., "Chemical analysis of the plasma-polymerized diphenyl thin films" Vacuum 57, 43-50, 2000.

[1.14] Sajeev, U. S., Mathai, C. J., Saravanan, S, Ashokan, R, Venkatachalam, S., Anantharaman, M. R., "On the optical and electrical properties of rf and a.c. plasma polymerized aniline thin films", Bull. Mater. Sci., **29**, No.2 (2006).

[1.15] Majumder, S. and Bhuiyan, A. H., "DC conduction mechanism in plasma polymerized vinylene carbonate thin films prepared by glow discharge technique", Polym. Sci. Ser. A, **53**(1), 85–91, (2011).

[1.16] Akther, H., Bhuiyan, A. H., "Space charge limited conduction in plasma polymerized N, N, 3, 5, tetramethylaniline thin films", Thin Solid Films, 488 (2005) 93-97.

[1.17] Blaszczyk-Lezak I., Aparicio F. J., Borra´s A., Barranco A., Alvarez-Herrero A., Ferna´ndez-Rodrı´guez M., Gonza´lez-Elipe A. R., "Optically active luminescent Perylene thin films deposited by plasma polymerization", J. Phys. Chem. C, 113, 431–438, 2009.

[1.18] Kipnusu, W. K. G. Katana, Migwi, C. M. I. Rathore, V. S. Sangoro, J. R., 'Charge transport mechanism in thin cuticles holding Nandi flame seeds', Int. J. Biomats. Vol. 2009, Article ID 548406.

[1.19] Olshausen, von. R., Sachs, Dr. Ing., Ing.,Dr., "AC loss and DC conduction mechanisms in polyethylene under high electric fields", IEE Proc., 128, Pt A, No. 3, 1981.

[1.20] Adnen Ltaief, Abdelaziz Bouazizi and Joel Davenas, 'Charge transport in carbon nanotubes-polymer composite photovoltaic cells', *Mater*, *2*, 710-718,(2009).

[1.21] Afroze, Tamanna., and Bhuiyan, A. H., "Electrical conduction mechanism in plasma polymerized 2-(diethylamino)ethyl methacrylate thin films", Polymer Engineering and Science 09/2015; DOI: 10.1002/pen.24161

[1.22] Motin, Rummana., and Bhuiyan, A. H., "Change in optical properties of as-deposited plasma polymerized 2, 6-diethylaniline thin Films due to iodine doping", J. Phys. Chem. Solids 75, 1179-1186, (1014)

[1.23] Afroze, Tamanna., and Bhuiyan, A. H., "Infrared and ultraviolet-visible spectroscopic studies of plasma polymerized 1,1,3,3-tetramethoxypropane thin films", Thin Solid Films, **519**, 1825–1830, (2011).

[1.24] Akther, H. and Bhuiyan, A. H., "Infrared and ultraviolet-visible spectroscopic investigation of plasma polymerized N,N,3,5–tetrametlylaniline thin films", Thin Solid Films, **474,** 14 – 18, (2005).

[1.25] Akther, H. and Bhuiyan, A. H., "Electrical and optical properties of plasma polymerized N, N, 3, 5 tetramethylamiline thin films", New J. Phys. 7**,** 173-176, (2005).

[1.26] Rahman, M. J. and Bhuiyan, A. H., "Structural and optical properties of plasma polymerized o-methoxyaniline thin films", Thin Solid Films, **534,** 132-136, (2013).

[1.27] Kamal, M. M. and Bhuiyan, A. H., "Optical characterization of plasma polymerized pyrrole-N,N, 3, 5 tetramethylaniline bilayer thin films", J. Appl. Polym. Sci, 121 (4), 2361–2368, (2011)

[1.28] Sajeev., and Anantharaman, M. R., "Determination of charge carrier transport in radio frequency plasma polymerized aniline thin films", J. Phys. D: Appl. Phys. **43,** 055403, (2010).

CHAPTER II

THEORETICAL BACKGROUND

2.1   Introduction

Different types of polymers and different polymerization processes are discussed in this chapter. The details of plasma, plasma polymerization, an overview of gas discharge plasma, plasma polymerization mechanism, different types of glow discharge reactors, advantages and disadvantages of plasma polymerized thin films are narrated in this chapter. Applications of plasma polymerized organic thin films are focused here. This chapter also includes the theories related to the different investigations.

2.2   Polymers

A polymer is a material whose molecules contain a very large number of repeat unites atoms/molecules linked by covalent bonds. Polymers are a large class of materials consisting of many small molecules called monomers that can be linked together to form long chains, thus they are known as macromolecules. Polymers consist mainly of identical or similar units joined together. The length of the polymer chain is specified by the number of repeat units in the chain, which is known as the degree of polymerization. Polymers having molecular weight roughly in the range of 1000-20,000 are called low polymers and those having molecular weight higher than 20,000 as high polymers [2.1, 2.2].

2.2.1   Some important types of polymers

There exist many polymers or macro-molecules, which contain hundreds or thousands of atoms. Some of these are naturally occurring and some of these are artificial. Both are covered a wide range of polymers.

Based on backbone chain, Polymers can be divided into two classes:
   a) <u>Organic Polymers</u>**:** A polymer whose backbone chain is essentially made of carbon atoms is termed as organic polymer. The most of synthetic polymers are organic.
   b) <u>Inorganic Polymers</u>: The molecules of inorganic polymers generally contain no carbon atom in their chain backbone. Silicone glass and rubber are examples of inorganic polymers.

Based on their origin polymers can be divided into two classes:
   a) <u>Natural Polymers</u>: Those isolated from natural materials are called natural polymers. Examples: Wool, Rubber, Silk, Leather, Cellophane, Cellulose Rayon

and so on.

b) <u>Synthetic Polymers:</u>   Industrially produced chemical substances consisting of a number of molecules linked together with covalent bonds are called synthetic polymers which has low molecular weight. Examples: Ploy Vinyl Chloride, Nylon, Polyethylene, Terylene, Synthetic fibers, etc.

c) <u>Semi-synthetic Polymers:</u> Semi-synthetic polymers are obtained from natural polymers by subjecting them to some chemical processes. eg: vulcanised rubber.

$$
\begin{array}{ccc}
CH_3 & & CH_3 \\
| & & | \\
CH_2 & & CH_2 \\
| & & | \\
-CH_2-CH-CH_2-CH_2-CH_2-CH_2-CH_2-CH-CH_2-
\end{array}
$$
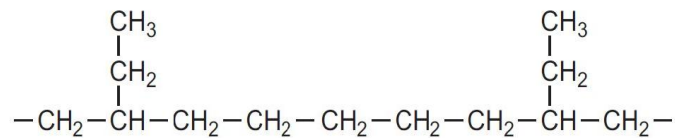
Fig. 2.1: Polymer chain structure of one of the simple polymers: poly (ethylene)

<u>Homopolymers</u>: consist of chains with identical bonding linkages to each monomer unit. This usually implies that the polymer is made from all identical monomer molecules. These may be represented as: -[X-X-X-X-X-X]-

<u>Copolymers</u>: consist of chains with two or more linkages usually implying two or more different types of monomer units. These may be represented as: -[X-Y-X-Y-X-Y-X]-

Depending on the different functional groups and structures in the field of macromolecules, polymers are classified in various ways listed in flowing table-2.1:

Table-2.1: Classification of Polymers

Basic Classification	Polymer Types
Origin	Natural, Synthetic, semi-synthetic
Line structure	Linear, Cross linked, Branched
Mode structure	Addition, Condensation
Tacticity	Atactic, Isotactic, Syndiotactic
Crystallinity	Crystalline, Semi-crystalline, Amorphous or Non-crystalline
Thermal response	Thermoplastic, Thermosetting

2.2.2   Crystalline and non-crystalline polymers

The morphology of most polymers is semi-crystalline. That is, they form mixtures of small crystals and amorphous materials and melt over a range of temperature instead of at a single melting point. There are some polymers that are completely amorphous, but most are a combination with the tangled and disordered regions surrounding the crystalline areas. Such a combination is shown in Fig 2.2

Amorphous   Crystalline   Semicrystalline
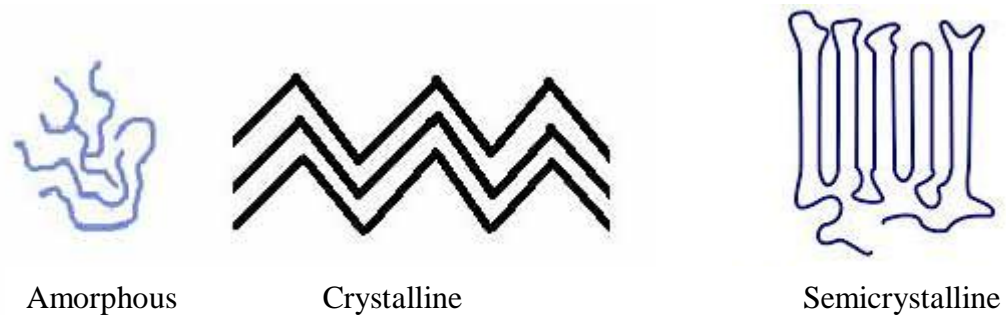
Fig. 2.2: Different states of polymers

An amorphous solid is formed when the chains have little orientation throughout the bulk polymer. The glass transition temperature is the point at which the polymer hardens into an amorphous solid. This term is used because the amorphous solid has properties similar to glass.

2.3 Polymerization Processes

Polymerization is a process of reacting monomer molecules together in a chemical reaction to form polymer chains or three-dimensional networks. There are many forms of polymerization and different systems exist to categorize them.

2.3.1 Addition polymerization

When a number of monomers undergo self-combination, resulting substance has a molecular mass many times larger than the monomer, the type of polymerization is known as "Addition polymerization". The empirical formula of addition polymer and the monomer is same. These reactions are catalyzed by peroxides or acids. Generally these reactions required a pressure of 100 atmosphere at 200 ^{0}C. Examples: polyethylene, polypropylene, polyvinyl chloride (PVC), Teflon.

Condensation polymers are formed by the combination of monomers with the elimination of simple molecules such as H_2O or CH_3OH.

There are two types of Condensation polymers:

1. Polyester,   2. Polyamide.

Examples: Nylon, terylene, Bakelite.

2.3.2 Conventional polymerization processes

Polymerization reactions can be classified into two major groups on the basis of the mechanism of growth reactions (reactions that lead to the increase in molecular weight or size of a polymer). These are (1) chain-growth polymerization and (2) step-growth polymerization. The addition and condensation polymers are nowadays also referred as chain growth polymers and step growth polymers depending on the type of polymerization mechanism they undergo during their formation.

2.3.3 Chain growth polymerization

In this type of polymerization, the molecules of the same monomer or different monomers add together on a large scale to form a polymer. The monomers used are unsaturated compounds, e.g., alkenes, alkadienes and their derivatives. This mode of polymerization leading to an increase in chain length or chain growth can take place through the formation of either free radicals or ionic species. However, the free radical governed addition or chain growth polymerization is the most common mode.

2.3.4 Step growth polymerization

This type of polymerization generally involves a repetitive condensation reaction between two bi-functional monomers. These polycondensation reactions may result in the loss of some simple molecules as water, alcohol, etc., and lead to the formation of high molecular mass condensation polymers. In these reactions, the product of each step is again a bi-functional species and the sequence of condensation goes on. Since, each step produces a distinct functionalized species and is independent of each other, this process is also called as step growth polymerization. The formation of terylene or dacron by the interaction of ethylene glycol and terephthalic acid is an example of this type of polymerization.

2.3.5 Radical polymerization

The most common type of addition polymerization is free radical polymerization. A free radical is simply a molecule with an unpaired electron. The tendency for this free radical to gain an additional electron in order to form a pair makes it highly reactive so

that it breaks the bond on another molecule by stealing an electron, learing that molecule with an unpaired election (which is another free radical). Free radicals are often created by the division of a molecule (known as an initiator) into two fragments along a single bond. Free radical polymerization is a method of polymerization by which a polymer is formed from the successive addition of free radical building blocks. Free radicals can be formed via a number of different mechanisms usually involving separate initiator molecules. Following creation of free radical monomer units, polymer chains grow rapidly with successive addition of building blocks onto free radical sites. Free radical polymerization is a key synthesis route for obtaining a wide variety of different polymers and material composites. The relatively non-specific nature of free radical chemical interactions makes this one of the most versatile forms of polymerization available and allows facile reactions of polymeric free radical chain ends and other chemicals or substrates. Free radical polymerization is a type of chain growth polymerization, along with anionic, cationic and coordination polymerization.

2.4   Plasma and Plasma Polymerization

2.4.1 Plasma: The fourth state of matter

The plasma is described as an electrically neutral medium of positive and negative particles. Plasma state is often referred to as the fourth state of matter. Much of the visible matter in the universe is in the plasma state. Stars, as well as visible interstellar matter, are in the plasma state. Besides the astro-plasmas, which are omnipresent in the universe, there are two main groups of laboratory plasma, i.e., the high-temperature plasma or fusion plasmas, and the so-called low temperature plasma or gas discharges. In general, a subdivision can be made between plasmas which are in the thermal equilibrium and those which are not in the thermal equilibrium. Thermal equilibrium implies that the temperature of all species (electrons, ions, neutral species) is the same. High temperature is required to form these equilibrium plasmas, typically ranging from 4000 to 20000 K. This is true for stars, as well as for fusion plasmas. On the other hand, interstellar plasma matter is typically not in thermal equilibrium. When the temperature is greater than 10000 K all molecules and atoms tend to become ionized.

Depending upon the frequency used, one decides thereby between alternating current (50 Hz), Audio (kHz)- Radio (MHz) frequency or microwave (GHz) plasmas. Plasmas

get used technically, i.e. in fluorescent tubes and, above all, in recent times in the surface techniques.
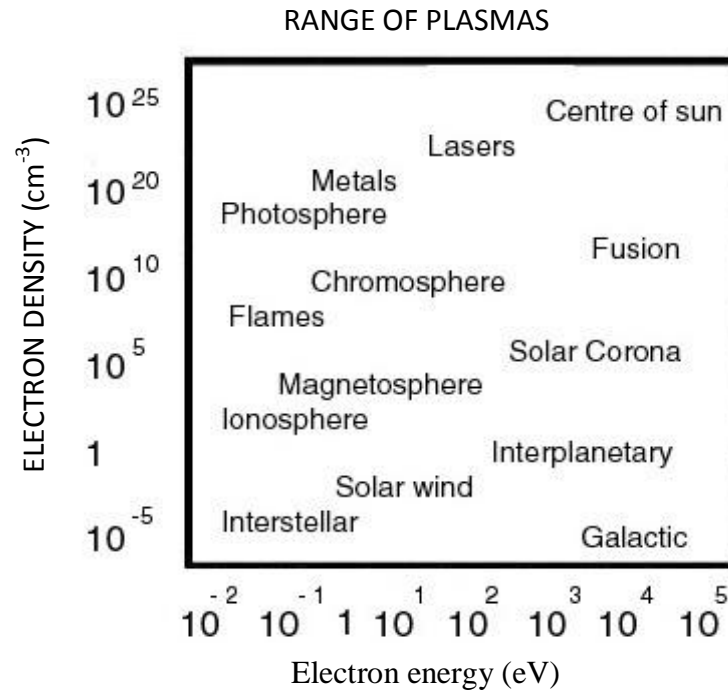
RANGE OF PLASMAS

Fig. 2.3: Schematic ranges of plasma.

In recent years, the field of gas discharge plasma applications has rapidly expanded [2.3, 2.4, 2.5]. Because of the multi- dimensional parameter space of the plasma conditions, there exists a large variety of gas discharge plasmas employed in a large range of applications. There are four types of plasma, i.e., (i) the glow discharge (GD), (ii) capacitively coupled (CC), (iii) inductively coupled plasma (ICP), and (iv) the microwave-inductively (MI) plasmas. However these plasmas, as well as related gas discharges, are more widely used in technological fields.

To generate plasma, it is necessary to ionize atoms or molecules in the gas phase. When an atom or molecules gains enough energy from an external excitation source or through collisions with another molecule, ionization occurs [2.6]. This happens usually when the molecules are under specific conditions, like extreme heat which generates the so-called hot plasmas, or under electrical glow discharge which generates the cold plasmas [2.7]. The plasmas loose energy to their surroundings through collision and radiation processes; as a result, energy must be supplied continuously to the system to maintain the plasma state. The easiest way to supply energy to a system in a continuous manner is with an electrical source. Therefore, electrical glow discharges are the most common plasmas [2.8].

2.4.2   An overview of gas discharge plasma

Plasma polymerization takes place in low temperature (or low pressure) plasma which is provided by a glow discharge operated in an organic gas or vapor (monomer) at low pressure between two electrodes. When a sufficient high potential difference is applied between the two electrodes, the gas will break into positive ions and electrons, giving rise to a gas discharge [2.4, 2.5].

The mechanism of the gas breakdown can be explained as follows; a few electrons are emitted from the electrodes due to the omnipresent cosmic radiation. However, when a potential difference is applied the electrons are accelerated by the electric field in front of the cathode and collide with the gas atoms. The most important collisions are the inelastic collisions leading to excitation and ionization. The excitation collisions create new electrons and ions. The ions are accelerated by the electric field toward the cathode, where they release new electrons by ion-induced secondary electron emission. The electrons give rise to new ionization collisions, creating new ions and electrons. These processes of electron emission at the cathode and ionization in the plasma make the glow discharge self-sustaining plasma [2.9].

Another important process in the glow discharge is the phenomenon of sputtering, which occurs at sufficiently high voltage. When the ions and fast atoms from the plasma bombard the cathode, they not only release secondary electrons, but also atoms of the cathode materials, which are called sputtering. The ions can be detected with a mass spectrometer and the excited atoms or ions emit characteristic photons, which can be measured with optical emission spectrometry. Alternatively, the sputtered atoms can also diffuse through the plasma and they can be deposited on a substrate, this technique used in materials technology (for the deposition of thin films).

2.4.3   Alternating current glow discharge

In an AC glow discharge, the mechanism depends on the frequency of the excitation. When the frequency of the applied voltage is more than a few kHz, positive ions become immobile and the positive space charge is partially retained from one half-cycle to the next (this helps the discharge to reinitiate). An increase of the frequency into MHz region causes that no significant displacement of either electrons or positive ions happens and losses of charged species from diffusion and recombination processes

are replaced by electron-impact ionization of neutral gas molecules in the discharge volume. This type of discharge is called rf glow discharge (100 kHz- 30 MHz). If the gaseous phase of monomer is subjected to an alternating electric field, the glow discharge is also achieved. But, the mechanism of glow discharge is changed with the frequency. At low frequencies(e.g., 50 Hz), the system can be looked upon as a dc glow discharge with alternating polarity. By increasing the frequency of the applied voltage, positive ions become immobile, because they can no longer follow the periodic changes in field polarity, and only respond to time - averaged fields. In radiofrequency plasma (13.56 MHz) therefore, no contact between the electrodes and the plasma is required. The plasma can be initiated and sustained by external electrodes, at a much lower voltage than is required for maintaining a direct current glow discharge [2.10, 2.11].

2.4.4 Direct current glow discharge

When a potential difference is applied between two electrodes, the gases (e.g. argon) will breakdown into electrons and positive ions. The latter can cause secondary electron emission at the cathode. The emitted electrons give rise to collision in the plasma, e.g. excitation (which is often followed by de-excitation with emission of visible light radiation, hence explaining the name of the "glow" discharge) and ionization (which creates new electrons and ions, and therefore makes the glow discharge self sustaining plasma). Another important process in the glow discharge is the phenomenon of sputtering, which occurs at sufficiently high voltages. When the ions and first atoms from the plasma bombard the cathode, they not only release secondary electrons but also atoms of the cathode material, which is called sputtering. A direct discharge can operate over a wide range of discharge conditions.

The pressure can vary from below 1 Pa to atmospheric pressure. The product of pressure and distance between the electrodes (PD) is a better parameter to characterize the discharge. A DC glow voltage can operate over a wide range of discharge conditions. For instance, at lower pressure, the distance between cathode and anode should be longer to create a discharge with properties comparable to these of high pressure with small distance. The discharge can operate in a rare gas most often argon or helium or in a reactive gas such H_2, O_2, N_2, SiH_4, CH_4, etc.

For DC glow discharge the mechanism involves the bombardment of the electron with positive ions resulting in the generation of secondary electrons. These in turn are accelerated away from the cathode until they have gained enough energy to ionize a molecule or atom by inelastic collision. Such ionization produces additional electrons and ions. An electron can transfer essentially all its energy to an atom or molecule by inelastic collision, but very little by elastic collision. This is a consequence of the fact that the mass of electron is almost negligible relative to the mass of atom or molecule.

2.4.5   Capacitively coupled radiofrequency discharges

The electrodes are conductive in a capacitive coupled radio frequency glow discharge, When one or both of the electrodes are non conductive, the electrodes will be charged up due to the accumulation of positive or negative charges ,and the glow discharge will extinguish .This problem can be overcomed by using an alternating voltage between the two electrodes, so that each electrode will act alternately as the cathode and anode and the charge accumulated during one half cycle will be at least partially neutralized by the opposite charge accumulated during the next half cycle. In practice, many rf glow discharge processes operate at 13.56 MHz, because this is a frequency allotted by international communications authorities at which one can radiate a certain amount of energy without interfering with communications. For plasma processing applications, capacitively coupled rf discharges, also called "rf-diodes" consist in the simplest case, of a vacuum chamber containing two planar electrodes separated by a distance of several cm.

2.4.6   Deposition of thin films by plasma polymerization

The polymer thin films deposited by plasma polymerization, is essentially a plasma enhanced chemical vapor deposition process. It refers to the deposition of polymer films due to the excitation of an organic monomer gas and subsequent deposition and polymerization of the excited species on the surface of a substrate. Polymers formed by plasma polymerization are, in most cases, branched and cross-linking. Plasma polymerization is characterized by several features: [2.4, 2.7]

- The properties of the plasma polymer are not only determined by the monomer being used, but also by the plasma parameters.

- Plasma polymers are not characterized by repeating units.
- The monomer used for plasma polymerization does not have to contain a functional group, such as a double bond.

2.4.7   Fundamental aspects of plasma polymerization

The ionization of molecule is first elementary step of plasma polymerization and is more complex than the ionization of an atom. Conventional polymerization is highly dependent on the structure of the monomer. However, in plasma polymerization, monomers and any organic compound without a polymerizable structure such as a double bond can polymerize. Plasma polymerization takes place through several reaction steps. In the initiation stage, free radicals and atoms are produced by collisions of electrons and ions with monomer molecules, or by dissociation of monomers adsorbed on the surface of the sample. Secondarily, the formation of the polymeric chain by the propagation of the reaction can take place both in the gas phase and on the substrate film. Finally, termination can also take place in the gas phase or at the polymer surface ending either with the final product or with a closed polymer chain.

The forms gas in an evaporator and is pumped into the vacuum chamber. In the plasma polymerization process, a monomer gas is pumped into a vacuum chamber where it is polymerized by plasma to form a thin film. A glow discharge initiates polymerization. The excited electrons created in the glow discharge ionize the monomer molecules. The monomer molecules break apart (fractionate) create free electrons, ions, exited molecules and radicals. The radicals absorb, condense and polymerize on the substrate.

The electrons and ions crosslink, or create a chemical bond, with the already deposited molecules, creating a harder, denser coating. A schematic plasma polymerization configuration is presented in Fig. 2.4. The materials   obtained by plasma polymerization are significantly different from conventional polymers and also different from most inorganic materials. Hence plasma polymerization should be considered as a method of forming new types of materials rather than a method of preparing conventional polymers.
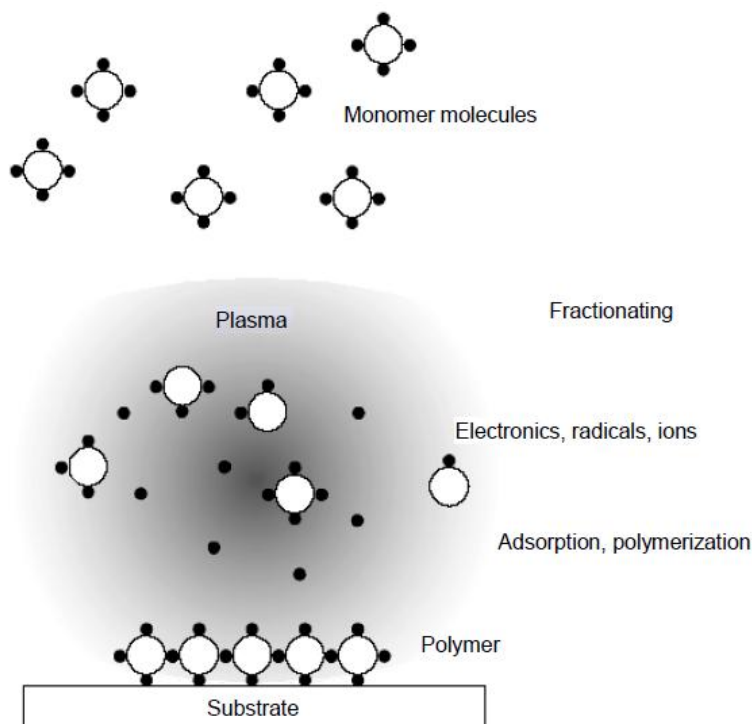
Fig. 2.4: A schematic plasma polymerization configuration

Comparison of the structures of plasma polymers and conventional polymers is shown in the Fig. 2.5. Plasma polymerization is a versatile technique for the deposition of films with functional properties suitable for a wide range of modern applications.

Conventional polymer   Plasma polymer
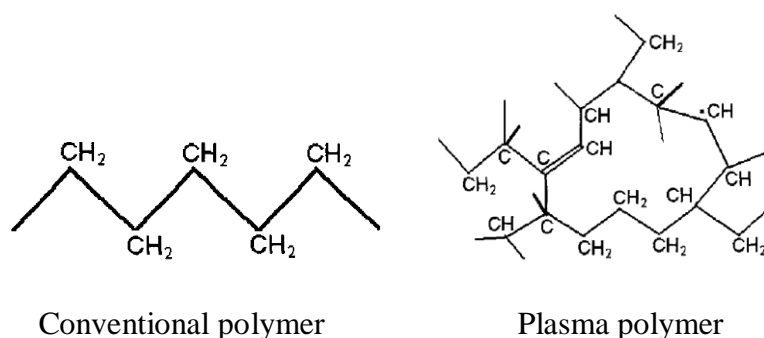
Fig. 2.5: Comparison of the structures of conventional polymers and plasma polymers.

To explain the reaction mechanism, many investigators discussed the effects of discharge conditions on polymerization rate such as polymerization time monomer pressure, discharge current, and discharge power and substrate temperature.

Though, same monomer is used for polymerization, polymers formed by plasma polymerization show distinguished chemical composition and chemical and physical properties from those formed by conventional polymerization. To appreciate the

uniqueness of plasma polymerization, it is useful to compare the steps necessary to obtain a good coating by a conventional coating process and by plasma polymerization. Coating a certain substrate with a conventional polymer, at least several steps are required (1) synthesis of a monomer, (2) polymerization of the monomer to form a polymer, (3) preparation of coating solution, (4) cleaning, (5) application of the coating, (6) drying of the coating and (7) curing of the coating. Polymers formed by plasma polymerization aimed at such a coating are in most cases branched and cross-linked [2.12-2.15].

2.4.8   Glow discharge reactors

One of the most important parts of plasma polymerization system is glow discharge reactor. Because reactor geometry influences the extent of charge particle bombardment on the growing films which affects the potential distribution in the system.

The most widely used reactor configurations for plasma polymerization can be broadly divided in to three classes [2.16]:

> (a) Bell jar reactors
>
> (b) Parallel plate electrode reactors and
>
> (c) Electrode less reactors

P   = Pumps
PS   = Power Supply
S   = Substrate
M   = Feed gas inlet
G   = Vacuum gauge
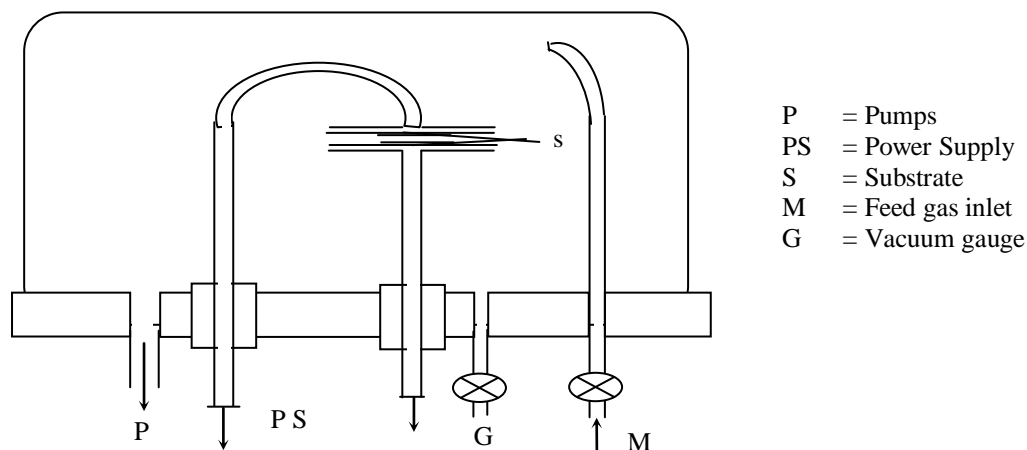
Fig. 2.6: Bell-jar reactor with parallel plate metal electrodes (internal reactor)

(a)   (b)
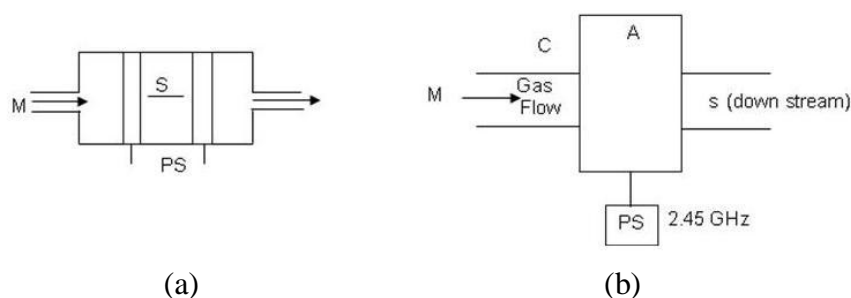
Fig. 2.7: a) Parallel plate internal electrode reactor and   b) Electrode less microwave

Reactors with internal electrodes have different names, e.g. flat bed parallel plates, planar, diode etc. Their main features are power supply, coupling system, vacuum chamber, rf driver electrode, grounded electrode, and eventually one or more substrate holders. Among the internal electrode arrangements a bell-jar-type reactor with parallel plate metal electrodes is mot frequently used by using ac (1-50 kHz) and rf fields for plasma excitation.
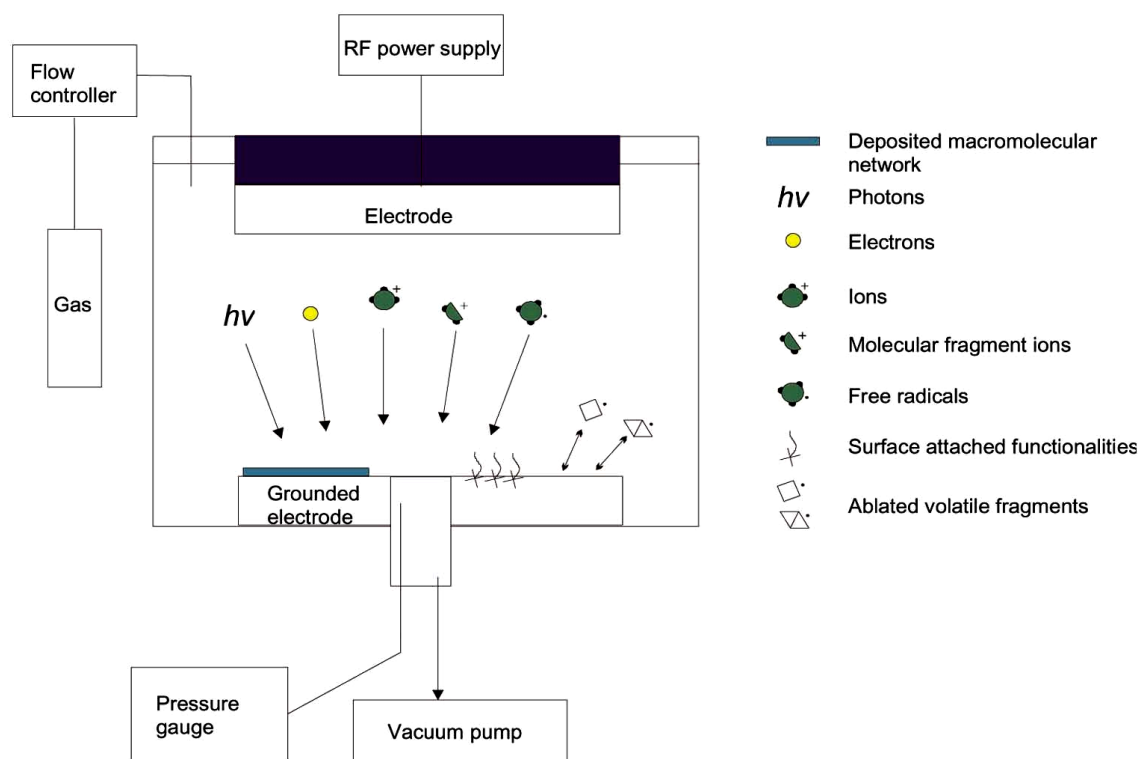
Fig. 2.8: A schematic diagram of the capacitively coupled parallel plate plasma reactor.

The vacuum chambers can be made either of glass or of conductive materials, such as metal. In the case of bell-jar reactors, no particular care is taken for the grounded electrode apart from its area. On the contrary, the design and arrangement of the

cathode require special attention: a metallic shield surrounding the electrode highly improves the glow confinement inside interelectrodic space; electrode material and area greatly affect the extension of sputtering on the target.

In the current research, capacitively coupled reactor (glow discharge plasma) system was used for the formation of thin films. Fig. 2.8 represents a scheme of a capacitively coupled parallel-plate plasma reactor, similar to the bell jar reactor. The possible species present when the plasma is generated are also drawn. Usually plasma reactor can use internal or external electrodes.

2.4.9   Overall reactions and growth mechanism in plasma polymerization

The mechanism of reaction by which plasma polymerization occurs is quite complex and cannot be specifically described for the general case. Operational parameters such as monomer flow rate, pressure frequency, and power affect the deposition rate and structure of the plasma film. The electrons or atoms generated by partial ionization of the molecules are the principle sources for transferring energy from the electric field to the gas in all glow discharges [2.17, 2.18].

In plasma polymerization, free electrons gain energy from an imposed electrical field and then transfer the energy to neutral gas molecules, which lead to the formation of many chemically reactive species. By applying greater power to the rf source, the energy per unit mass of the monomer is increased and may bring about changes in the fragmentation process. As a result, free radicals may become entrapped in the plasma-polymerized film and increase in concentration with increasing rf power. The deposition of polymer films in low-pressure plasma is a complex phenomenon involving reactions, which occur both in the plasma phase and at the surfaces bounding the plasma.

The study of plasma polymerization kinetics is commonly employed to elucidate polymerization mechanisms. With this background a comparison of the polymer formation rates of various monomers by plasma polymerization would provide an overview of the kind of reaction mechanism responsible for plasma polymerization.

The probable chain growth polymerization is represented by

$$M_n^* + M \quad \rightarrow \quad M_{n+1}^*$$
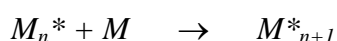
Where M_n* is the reactive chain carrying species and M is the monomer molecules. But Yasuda and Lamaze [2.18], on the basis of their observation on plasma polymerization ruled out the chain growth polymerization. The rapid step-growth mechanism is very likely to be the reaction in plasma polymerization and this reaction is expressed as:

$$[M_m*+M_n* \rightarrow M_{m+n}*] \times N$$
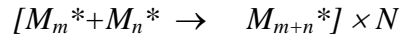
Where, N represents the number of repetitions of similar reactions. In this case, the reaction occurs between molecules.

In case of difunctional reactive species, $*M*$ the overall polymerization can be represented by

$$n*M* \rightarrow *(M_n)*$$
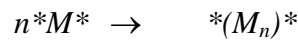
If the reactive species are monofunctional $(M*)$, such as free radical $R*$, the reaction is given by

$$M_m*+M_n* \rightarrow M_{m+n}$$
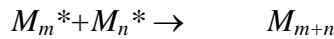
This is essentially a termination process that occurs in free radical polymerization and does not contribute without additional elementary steps. Yasuda and Lamaze [2.20] pointed out that the reactivation of the product of an elementary reaction was bound to occur in plasma.
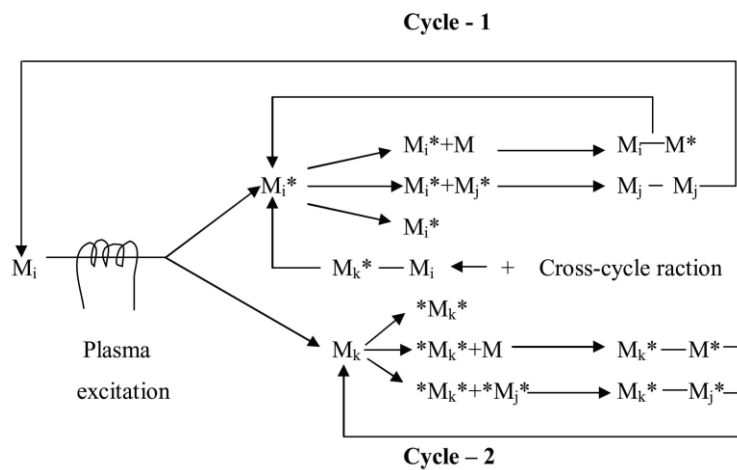
Fig. 2.9: Schematic representation of bicycle step growth mechanism of plasma polymerization

The overall polymerization mechanism based on the rapid step-growth principle shown in Fig. 2.9. The figure shows the overall reaction, which contains two major routes of rapid step-growth. Cycle-1 is via the repeated activation of the reaction products from monofunctional activated species, Cycle-2 is via difunctional or multifunctional activated species.

Here, M_x refers to neutral species that can be original monomer molecule or any of the dissociation products including some atoms, such as hydrogen, chlorine, fluorine and others; M* activated species; *M** difunctional activated species and the subscripts i, j, k indicate the difference in the size of the species involved (i=j is possible, thus i=j=1 for initial monomer.)

2.4.10 Advantages and disadvantages of plasma polymerization

The plasma polymerization process is a completely dry process and the deposition is flaw less. The plasma polymerization is capable of forming an ultra-thin, uniform and pinhole-free film containing a minimal amount of flaw. No catalytic agent is required to form polymers. The technique is preferred in many cases over conventional polymerization process due to the absence or minimization of undesirable by-products. An important contribution to the field of plasma polymerization is that one plant production unlike conventional polymers plasma polymers do not consist of chains with a regular repeat unit but tend to form an irregular three dimensional cross-linked network. Plasma-polymerization films are generally chemically inert, insoluble, mechanically tough, and thermally stable and have been used in a wide variety of applications such as protective coatings electrical optical and biomedical films [2.19, 2.20].

The main disadvantages of the plasma polymerization are-

i)   Low deposition rates. Only very thin films can be deposited economically on high production items. Contamination can be a problem and care must be exercised to prevent extraneous gases, grease films, and pump oils from entering the reaction zone.

ii)   The chemistry produced on a surface is often not well defined, sometime a complex branched hydrocarbon polymer will be produced.

Plasma polymerization is far well developed process for many types of modification that simply cannot be done by any other technique.

The advantages of Plasma Polymers are-

i)   <u>Pinhole-free</u>: Under common reaction conditions, the plasma film appears to coalesce during formation into a uniform over layer free of voids. Transport property and electrical property studies suggest this continuous barrier structure.

ii)   <u>Unique substrates</u>: Plasma-deposited polymeric films can be placed upon almost any solid substrate including metals, ceramics, and semiconductors. Other surface grafting or surface modification technologies are highly dependent upon the chemical nature of the substrate.

iv)   <u>Barrier film</u>: The pinhole-free and dense, cross-linked nature of these films suggests they have potential as barrier and protective films

vi)   <u>Good adhesion to the substrate</u>: The energetic nature of the gas phase species in the plasma reaction environment can induce some mixing and implantation between the film and the substrate.

2.4.11 Applications of plasma-polymerized organic thin films

A large number of applications have been proposed in terms of plasma modification of polymers and thin film deposition. Typical uses of plasma treatment and plasma polymerization are listed in Table 2.2.

Table-2.2: Application of plasma polymerized thin films

Electronics	Amorphous semiconductor, amorphous fine ceramic etching, IC
Electrical	Thin film dielectrics, Insulator, separation membrane for batteries
Chemical processing	Reverse osmosis membrane, permselective membrane, insolubilization
Optical	Anti-reflection coating, anti-dimming coating, optical fiber. Optical waveguide laser, contact lens
Surface modification	Adhesive improvement, protective coating, abrasion-resistant coating
Textile	Anti-flammability, anti-electrostatic treatment, dyeing affinity, water- repellence
Biomedical	Immobilized enzymes, sterilization & Pasteurization

2.5   Field Emission Scanning Electron Microscopy

Field emission scanning electron microscopy (FESEM) is a method for high-resolution imaging of surfaces. It is the mostly used technique to obtain surface morphological information of plasma polymerized thin films. The combination of higher magnification, larger depth of focus, greater resolution and ease of sample observation makes FESEM one of the most widely used instruments in research areas. It uses electrons instead of light to form an image. By heating of a metallic filament, a beam of electrons is produced at the top of the microscope. The electron beam follows a vertical path through the column of the microscope. It makes its way through electromagnetic lenses which focus and direct the beam down towards the samples. The primary electrons enter a surface with an energy of $0.5 - 30$ kV and generate many low energy secondary electrons. In addition to low energy secondary electrons, backscattered electrons and X-rays are generated by primary electron bombardment. The intensity of backscattered electrons can be correlated to the atomic number of the element within the sampling volume. Hence, some qualitative elemental information can be obtained. Detectors collect these secondary or back scattered electrons, and convert them to a signal, that is sent to a viewing screen. The intensities of the emitted secondary electrons vary with topography and be detected and displayed using a cathode ray tube screen, producing a detailed image of the surface. FESEM, accompanied by X-ray analysis, is considered a relatively rapid, inexpensive, and basically non-destructive approach to surface analysis. It is often used to survey surface analytical problems before proceeding to techniques that are more surface-sensitive and specialized. Energy dispersive analysis of X-ray referred to as EDAX or EDS, is an X-ray technique used to identify the elemental composition of materials. Applications include materials and product research, troubleshooting, deformulation, and etc. The analysis of characteristic X-rays (EDAX analysis) emitted from the sample gives more quantitative elemental information.

Electron gun

Electron beam

Anode

Magnetic lens

Scanning coils

Back scattered
electron detector

Secondary electron
detector

Specimen

Stage

To Monitor
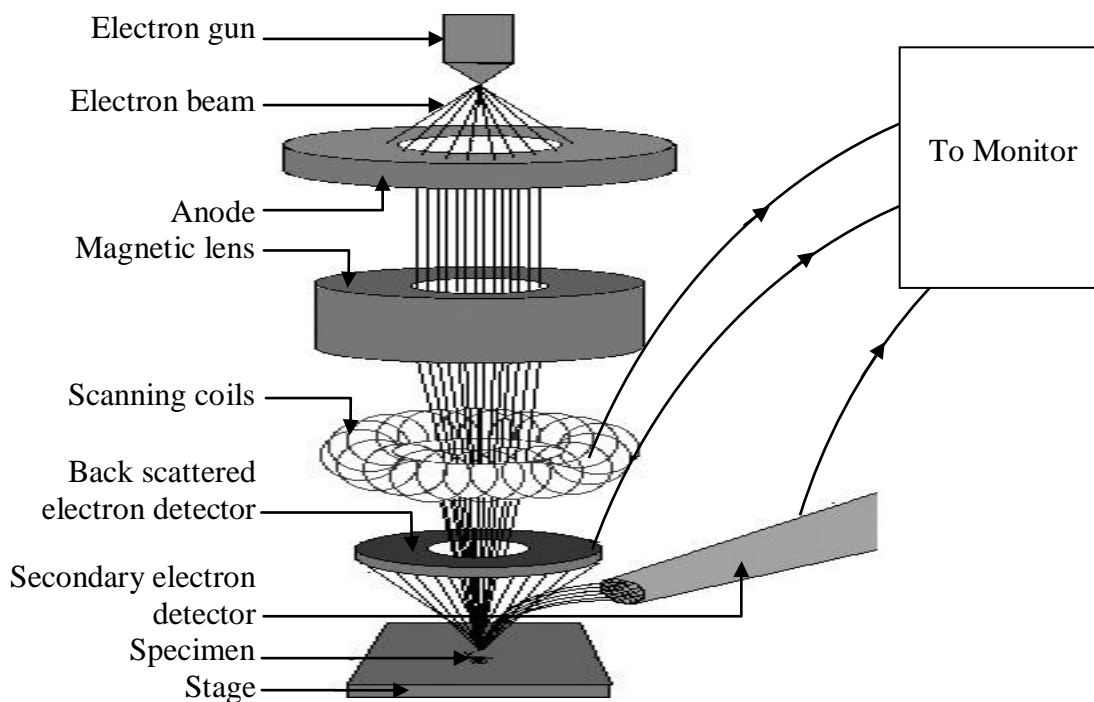
Fig. 2.10: Schematic diagram of a field emission scanning electron microscope

2.6   Introduction to Infrared Spectroscopy

The main goal of Infrared (IR) spectroscopic analysis is to determine the chemical functional groups in a material. Different functional groups absorb characteristic frequencies of IR radiation and this absorption results due to the changes in vibrational and rotational status of the molecules. Actually, a molecule, when exposed to radiation produced by the thermal emission of a hot source (a source of IR energy), absorbs only at frequencies corresponding to its molecular modes of vibration in the region of the electromagnetic spectrum between visible (red) and short waves (microwaves). These changes in vibrational motion give rise to bands in the vibrational spectrum; each spectral band is characterized by its frequency and amplitude. The absorption frequency depends on the vibrational frequency of the molecules, whereas the absorption intensity depends on how effectively the IR photon energy can be transferred to the molecule, and this depends on the change in the dipole moment that occurs as a result of molecular vibration. As a consequence, a molecule will absorb IR radiation only if the absorption causes a change in the dipole moment. Thus, all compounds except for elemental diatomic gases such as N_2, H_2 and O_2, have IR spectra and most components

present in a flue gas can be analyzed by their characteristic IR absorption. Its principal strengths are:

(i) It is a quick and relatively cheap spectroscopic technique,

(ii) An IR spectrum of a given compound is unique and can therefore serve as a fingerprint for this compound &

(iii) It is useful for identifying certain functional groups in molecules.

2.6.1   Infrared frequency range and spectrum presentation

IR radiation spans a section of the electromagnetic spectrum having wave-numbers from roughly 3000 to 10 cm^{-1}, or wavelengths from 0.78 to 1000 µm. IR absorption positions are generally presented as either wave numbers ($\bar{\nu}$) or wavelengths (λ). Thus, wave-numbers are directly proportional to frequency, as well as the energy of the IR absorption. In contrast, wavelengths are inversely proportional to frequencies and their associated energies. Wave numbers and wavelengths can be inter-converted using the following equation:

$$\bar{\nu}(cm^{-1}) = \frac{1}{\lambda(\mu m)} \times 10^4 \quad .... \quad (2.1)$$

Absorbance, $A = \log_{10}(1/T) = \log_{10}(I_0/I)$ ....(2.2)

Whose T is transmittance, I_0 is incident radiation and I is emergent radiation.

Table 2.3: Three smaller areas in IR region

	Near IR	Mid IR	Far IR
Wavenumber (cm^{-1})	13000 – 4000 cm^{-1}	4000 – 200 cm^{-1}	200 – 10 cm^{-1}
Wavelength (µm)	0.78 – 2.5 µm	2.5 – 50 µm	50 – 1000 µm

The IR region is commonly divided into three smaller areas: near IR, mid IR, and far IR. These are shown in Table 2.3 the region of most interest for chemical analysis is the mid-infrared region (4,000 cm^{-1} to 400 cm^{-1}) which corresponds to changes in vibrational energies within molecules.

2.6.2   Type of infrared absorption

The major types of molecular vibrations are stretching and bending. The various types of vibrations are illustrated in Fig. 2.11 and Fig. 2.12. IR radiation is absorbed and the

associated energy is converted into these types of motions. The absorption involves discrete, quantized energy levels. However, the individual vibrational motion is usually accompanied by other rotational motions. These combinations lead to the absorption bands, not the discrete lines, commonly observed in the mid IR region.

Stretching: Change in inter-atomic distance along bond axis. There are two types of Stretching vibrations: Symmetric and Asymmetric.

Symmetric   Asymmetric
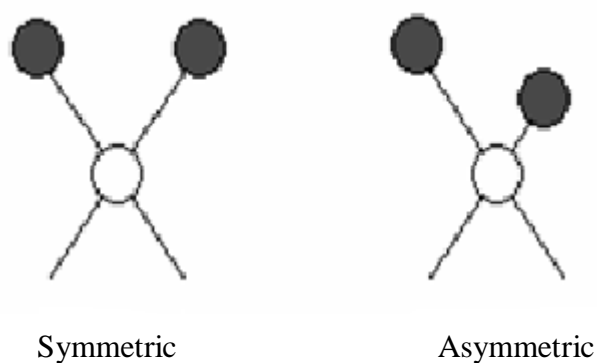
Fig. 2.11: Stretching vibrations

Bending: Change in angle between two bonds. There are four types of bend: Rocking, Scissoring, Wagging and Twisting.
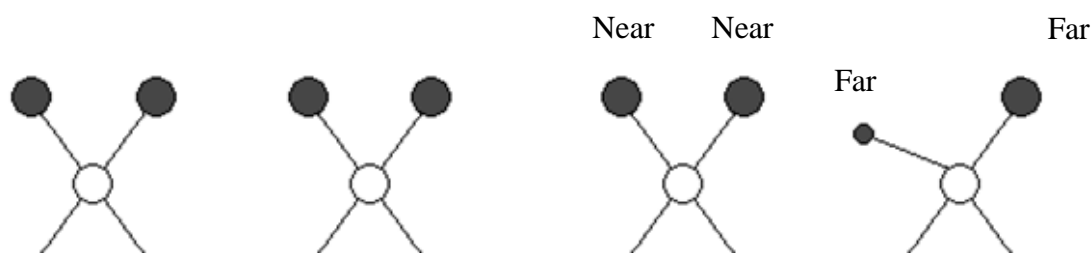
In plane   rocking   In plane   scissoring   Out of plane   wagging   Out of plane   twisting

Fig. 2.12: Bending vibrations

In general, a polyatomic molecule with n atoms has $3n - 6$ distinct vibrations. Each of these vibrations has an associated set of quantum states and in IR spectroscopy the IR radiation induces a jump from the ground (lowest) to the first excited quantum state. Although approximate, each vibration in a molecule can be associated with motion in a particular group.

2.7   Thermal Analysis

2.7.1   Differential thermal analysis

In DTA, the material under study and an inert reference are made to undergo identical thermal cycles, while recording any temperature difference between sample and reference. This differential temperature is then plotted against time, or against temperature (DTA curve, or thermogram). Changes in the sample, either exothermic or endothermic, can be detected relative to the inert reference. Thus, a DTA curve provides data on the transformations that have occurred, such as glass transitions, crystallization, melting and sublimation. The area under a DTA peak is the enthalpy change and is not affected by the heat capacity of the sample.
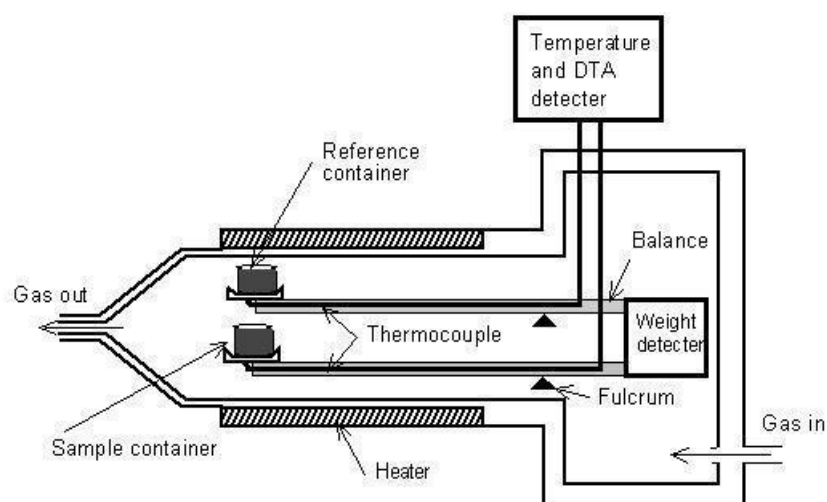
Fig. 2.13: Schematic diagram of the DTA system

The exothermic and endothermic reactions are generally shown in the DTA traces as positive and negative deviations respectively from a base line. So DTA offers a continuous thermal record of reactions in a sample. The areas under the bands or peaks of DTA spectra are proportional to the amount of heat absorbs or evolved from the sample under investigation, where temperature and sample dependent thermal resistance are the proportionality factors. Thus DTA is needed primarily for the measurement of transition temperature.

2.7.2   Thermogravimetric analysis

In TGA, changes in weight of a material masers as a function of temperature (or time) under a controlled atmosphere. Its principal uses include measurement of a material's

thermal stability and composition. TGA instruments are routinely used in all phases of research, quality control and production operations.
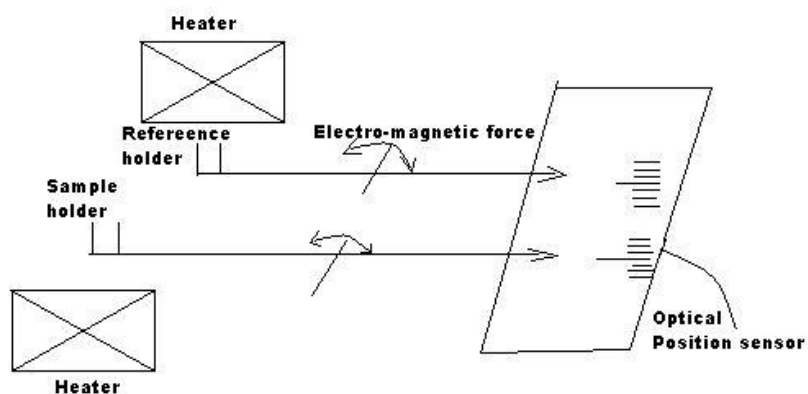
Fig. 2.14: Schematic diagram of the TGA system

2.8   Ultraviolet-Visible Spectroscopy

The wavelength of light that a compound absorbs is the characteristic of its chemical structure. Specific regions of the electromagnetic spectrum are absorbed by exciting specific types of molecular and atomic motions to higher energy levels. Absorption of visible and ultraviolet (UV) radiation is associated with excitation of electrons, in both atoms and molecules, to higher energy states. Most molecules required very high energy radiation. Light in the UV-visible (UV-Vis) region is adequate for molecules containing conjugated electron systems and as the degree of conjugation increases, the spectrum shifts to lower energy.
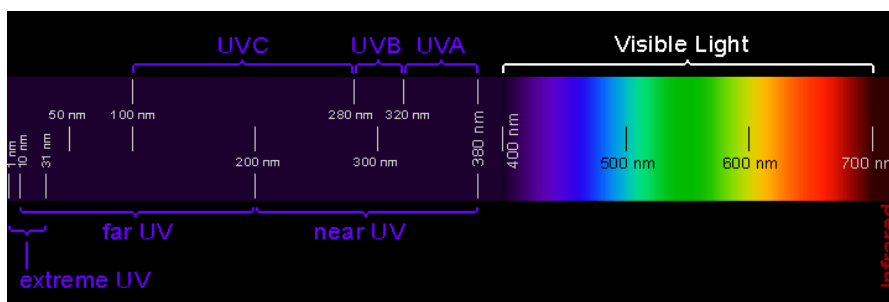
Fig 2.15: Light Spectrum

Possible electronic transitions of π, σ, and n electrons are:

$\sigma \rightarrow \sigma^*$ *transitions*: An electron in a bonding σ orbital is excited to the corresponding antibonding orbital. The energy required is large. For example, methane (which has only C-H bonds, and can only undergo $\sigma \rightarrow \sigma^*$ transitions) shows an absorbance maximum at 125 nm. Absorption maxima due to $\sigma \rightarrow \sigma^*$ transitions are not seen in typical UV-Vis. spectra (200 - 700 nm).

$n \rightarrow \sigma^*$ *Transitions*: Saturated compounds containing atoms with lone pairs (non-bonding electrons) are capable of $n \rightarrow \sigma^*$ transitions. These transitions usually need less energy than $\sigma \rightarrow \sigma^*$ transitions. They can be initiated by light whose wavelength is in the range 150 - 250 nm. The number of organic functional groups with $n \rightarrow \sigma^*$ peaks in the UV region is small.

$n \rightarrow \pi^*$ *and* $\pi \rightarrow \pi^*$ *Transitions*: Most absorption spectroscopy of organic compounds is based on transitions of *n* or π electrons to the π^* excited state. This is because the absorption peaks for these transitions fall in an experimentally convenient region of the spectrum (200 - 700 nm). These transitions need an unsaturated group in the molecule to provide the π electrons.
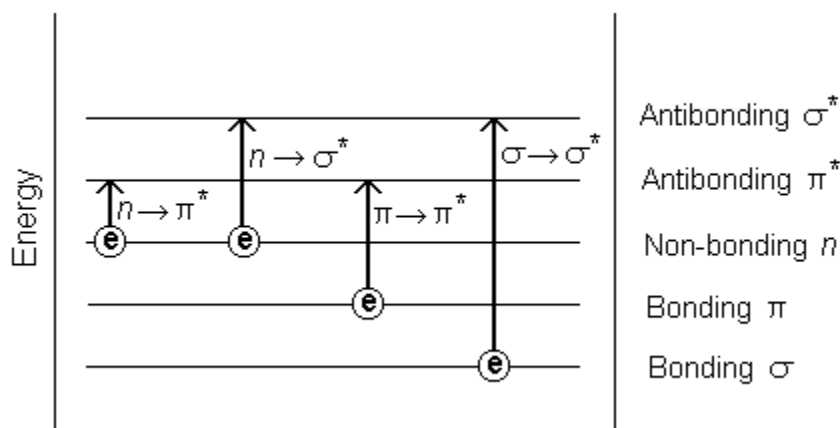
Fig. 2.16: Summary of electronic energy levels

The solvent in which the absorbing species is dissolved also has an effect on the spectrum of the species. Peaks resulting from $n \rightarrow \pi^*$ transitions are shifted to shorter wavelengths (*blue shift*) with increasing solvent polarity. Often (*but not always*), the reverse (i.e. *red shift*) is seen for $\pi \rightarrow \pi^*$ transitions. This is caused by attractive polarization forces between the solvent and the absorber, which lower the energy levels of both the excited and unexcited states.

2.8.1   Direct and indirect optical transitions

Materials are capable of emitting visible luminescence when subjected to some form of excitation such as UV light. The *E-k* diagrams for a direct band gap material and an indirect gap material is schematically illustrated in Fig. 2.17, where *E* and *k* are respectively the kinetic energy and wave vector of the electron or hole ($E = k^2\hbar^2/2m$, where $\hbar = h/2\pi$ and *m* is the electron or hole effective mass).

The shaded states at the bottom of the conduction band and the empty states at the top of the valence band respectively represent the electrons and holes created by the absorption of an UV or visible photon with an energy $\hbar\omega_{exc}$ exceeding the band gap E_g of the material, an electron-hole pair is created and the electron (hole) is excited to states high up in the conduction (valence) band.
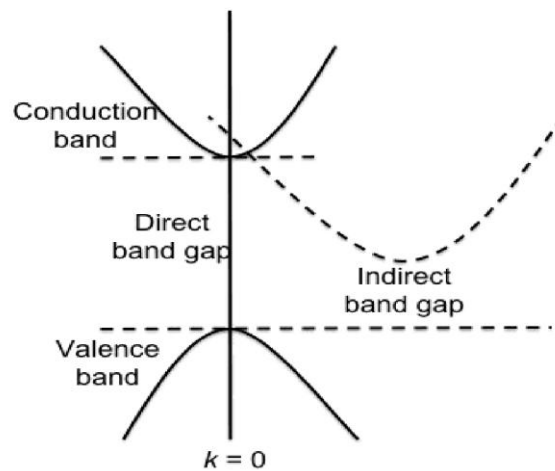
Fig. 2.17: Schematic band diagrams for the photoluminescence processes in a direct gap material (*left*) and an indirect gap material (*right*).

In a direct gap material, the valence band maximum and the conduction band minimum occur at the same *k* values which imply that the electron wave vector should not change significantly during a photon absorption process. This is represented by photon absorption and emission processes by vertical arrows on *E-k* diagrams.

In contrast, for an indirect band gap material, of which the conduction band minimum and the valence band maximum have different *k* values, conservation of momentum implies that the photon absorption process must be assisted by either absorbing (indicated by a "+" sign) or emitting (indicated by a "-" sign) a phonon (a quantum of lattice vibration), because the electron wave vector must change significantly in

jumping from the valence band in state (E_i, $\vec{\mathbf{k}}_i$) to a state (E_f, $\vec{\mathbf{k}}_f$) in the conduction band, and the absorption of a photon alone can not provide the required momentum change since $\left|\vec{\mathbf{k}}_{phot}\right| << \left|\vec{\mathbf{k}}_i - \vec{\mathbf{k}}_f\right|$.

2.8.2 The Beer-Lambert law

This method is most often used in a quantitative way to determine concentrations of an absorbing species. For most spectra the solution obeys Beer's law. This tells us that the light absorbed is proportional to the number of absorbing molecules. And Lambert's law states that the fraction of radiation absorbed is independent of the intensity of the radiation. Combining these two laws called Beer-Lambert law. Using Beer-Lambert law, the absorption spectrum can be analyzed [2.21], which governs the absorption of light by the molecules. It states that, "When a beam of monochromatic radiation passes through a homogeneous absorbing medium the rate of decrease in intensity of electromagnetic radiation in UV-Vis region with thickness of the absorbing medium is proportional to the intensity coincident radiation". If I_o is the intensity of the incident light, I is the intensity of the transmitted light

$$I = I_0 e^{-\alpha d} \quad \dots\dots\dots\dots\dots\dots\dots\dots\dots\dots\dots\dots\dots\dots\dots\dots\dots\dots\dots(2.3)$$

$$ln\left(\frac{I_0}{I}\right) = \alpha d \quad \dots\dots\dots\dots\dots\dots\dots\dots\dots\dots\dots\dots\dots\dots\dots (2.4)$$

Where α the absorption coefficient and d is is the path length of the absorbing species.

The absorption co-efficient (α) can be calculated from the absorption data as [2.47, 2.48]

$$\alpha = \frac{2.303A}{d} \quad \dots\dots\dots\dots\dots\dots\dots\dots\dots\dots\dots\dots\dots\dots\dots (2.5)$$

Where absorbance, $A = \log_{10}\left(\frac{I_0}{I}\right)$

The relation between absorption co-efficient (α) and the molar absorptivity or extinction co-efficient (k) is

$$\alpha = \frac{4\pi k}{\lambda} \quad \dots\dots\dots\dots\dots\dots\dots\dots\dots\dots\dots\dots\dots\dots\dots (2.6)$$

Here λ is the wavelength.

To estimate the nature of absorption a random phase model is used where the momentum selection rule is completely relaxed. The integrated density of states $N(E)$ has been used and defined by

$$N(E) = \int_{-\infty}^{+\infty} g(E)dE \dots\dots\dots\dots\dots\dots\dots\dots\dots\dots\dots\dots\dots\dots\dots(2.7)$$

The density of states per unit energy interval may be represented by $g(E) = \dfrac{1}{V} \sum \delta(E - E_n)$, where V is the volume, E is energy at which $g(E)$ is to be evaluated and E_n is the energy of the nth state.

If $g_v \propto E^p$ and $g_c(E) \propto (E-E_{opt})^q$, where energies are measured from the valance band mobility edge in the conduction band (mobility gap), and substituting these values into an expression for the random phase approximation, the relationship obtained $v^2 I_2(v) \propto (hv-E_o)^{p+q+1}$, where $I_2(v)$ is the imaginary part of the complex permittivity. If the density of states of both band edges is parabolic, then the photon energy dependence of the absorption becomes $\alpha v \propto v^2 I_2(v) \propto (hv-E_{opt})^2$. So for higher photon energies the simplified general equation is

$$\alpha h v = b(hv - E_{opt})^n \dots\dots\dots\dots\dots\dots\dots\dots\dots\dots\dots\dots\dots\dots..(2.8)$$

Where hv is the energy of absorbed radiation, n is the parameter connected with distribution of the density of stales and b is the proportionality factor. The index $n = 1/2$ for direct transition and $n=2$ for indirect transition energy gaps respectively [2.22, 2.23].

Thus, from the straight-line plots of $(\alpha h v)^2$ versus hv and $(\alpha h v)^{1/2}$ versus hv the direct and indirect energy gaps of insulators and/or dielectrics can be determined.

The Beer-Lambert law has implicit assumptions that must be met experimentally for it to apply otherwise there is a possibility of deviations from the law to be observed [2.24].

2.9   Direct Current Electrical Conduction Mechanism

2.9.1   Introduction

In the dc electrical conduction in plasma-polymerized materials, the carriers may either be electronic or ionic in nature and conduction is considered through the film, rather than along the plane of the film. The low field properties, which are usually ohmic in nature, but the high field electrical properties cannot describe by a single conduction process; usually various field strength ranges manifest different electrical conduction phenomena. This chapter includes the short description of the existing theories of DC electrical conduction mechanisms which are usually operative in thin insulating polymer and other thin films and the experimental techniques used in the measurements of current J-V and thermally activated current to ascertain the conduction mechanism operative in the investigated PP(OMA-TMA) thin films.

2.9.2   DC electrical conduction mechanism

Electrical properties of insulating polymers are there responses when an electric field is applied to them. The subject of electrical properties of polymers covers an extremely diverse range of molecular phenomena. In contrast to metals, in which the electrical field response is one of electronic conduction, polymers may respond in a more varied manner, and a whole set of delicate electrical effects may be observed. No known polymer is completely free of conduction processes, however small the quantity of charge carriers it may possess. Low level conduction in insulating polymers can take a variety of forms. Conduction may very often be contributed by impurities that provide a small concentration of charge carriers in the form of electrons or ions. At high fields, the electrodes may inject new carriers (holes and electrons) into polymers. At very high fields, these and other processes will lead to complete breakdown of polymers as insulating materials. The imposition of an electrical field upon a polymer will cause a redistribution of any charges in the polymer, provided they are mobile enough to respond in the time scale in the applied field. If some of the mobile charges are able to diffuse throughout the specimen and charge migration through the electrode sample interface is possible, then the charges will support a dc conductance. It should be mentioned that the vacuum-deposited thin film insulators can contain a large density of

both impurity and trapping centers. The dc conduction mechanisms in different plasma-polymerized thin films have reported is the following:

A well judged study of electrical conduction in vacuum deposited thin films cannot be accomplished without consideration of these possibilities [2.25]. A power law can express the variation of current density with voltage in a material generally:

$$J \propto V^n \qquad \text{.. (2.9)}$$

Where, n is a power factor. When n is unity, the conduction is ohmic. If the value of n is less or more than unity, then the conduction process is other than ohmic. Many scientists have investigated three worth-mentioning electrical conduction mechanisms which are operative in the thin films of various organic compounds [2.26-2.41]:

- The injection of carriers from the electrode by means of thermal or field assisted emission usually referred to as *Schottky* emission.

- The other process in which carriers are produced by the dissociation of donor-acceptor centers in the bulk of the material, is called *Poole-Frenkel* generation.

- If the generation process is slower than transport by the carriers through the material, the conduction is controlled by generation, specifically by either the Schottky, or PF mechanism. Conversely, when the transport is slower than generation, it constitutes the rate-determining step, and the conduction is described by the theory of SCLC. The phenomenon is, if a charge is injected at the electrode polymer interface, a large excess carrier density at the injecting electrode will exist and an SCLC will flow [2.25, 2.26].

2.9.3   Space charge limited conduction mechanism

When an Ohmic contact is made to the insulator, the space charge injected into the conduction band of the insulator is capable of carrying current and when the transport is slower than generation, it constitutes the rate-determining step, and the conduction is described by the theory of SCLC [2.25].

When a voltage bias is applied to the metal electrodes, this results an addition of positive charge to the anode and negative charge to the cathode. If now the voltage bias increases, the net positive charge on the anode increases and that on the cathode decreases. Assuming that the anode region extends throughout the insulator and neglecting the diffusion effect the current can be interpreted by the Mott and Gurney relation

$$J = \frac{9\mu\varepsilon'\varepsilon_0 V^2}{8d^3} \qquad \text{.. (2.10)}$$

Where, μ is the mobility of charge carriers, ε is dielectric constant, ε_0 is the permittivity of free space, V is the applied voltage and d is the thickness.
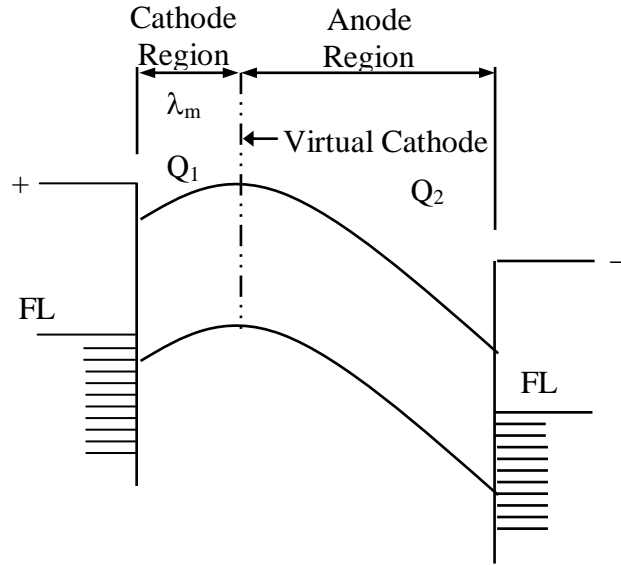
Fig. 2.18: Energy diagram for different regions under space charge limited conduction mechanism.

If the insulator contains N_t shallow traps positioned an energy E_t below the conduction band then the free component of the space charge

$$\rho_f = eN_c \exp\left(-\frac{E_F}{kT}\right) \qquad \text{.................................. (2.11)}$$

and trapped component of space charge

$$\rho_t = eN_t \exp\left(-\frac{E_t}{kT}\right) \qquad \text{.................................. (2.12)}$$

thus trapping factor, θ is defined as

$$\theta \equiv \frac{\rho_f}{\rho_t} = \frac{N_c}{N_t} \exp\left(-\frac{E_t}{kT}\right) \qquad \text{.................................. (2.13)}$$

Where N_c is the effective density of states in the conduction band, and N_t the density of trapping levels situated at an energy Es below the conduction band edge.

The SCLC current density with traps is defined by

$$J = \frac{9\mu\varepsilon'\varepsilon_0 V^2}{8d^3}\theta \qquad \text{.. (2.14)}$$

For a shallow trap SCLC and trap-free SCLC, $\theta = 1$. According to Eq^n (2.14), J varies as d^{-1} in the Ohmic region and as d^{-3} in the SCLC region for the trap-filled SCLC part. For a fixed V, the dependence of ln J on ln d should be linear with slope $l \geq -3$.

Lampert calculated the voltage at which the transition from the Ohmic to shallow trap SCLC region (V_{tr}) occurs is given by

$$V_{tr} = \frac{8}{9} n_0 \frac{ed^2}{\varepsilon}$$ ……………………………………. (2.15)

Where, volume generated free carrier density, n_0 is independent of both μ and J [2.42]. According to Fig. 2.19 it was found that the second linear region would extend up to a certain voltage, called as the crossover voltage, and beyond which the current would vary with the voltage as a power law:

$$I \propto V^2$$ ……………………………………. (2.16)

Which would continue until the current is close to the saturation current, i.e. the maximum current that the electrode could supply. However in real samples which contain several trap sites to capture the electrons that had been injected inside the sample. There are two types of traps; the ones above the Fermi level are the shallow
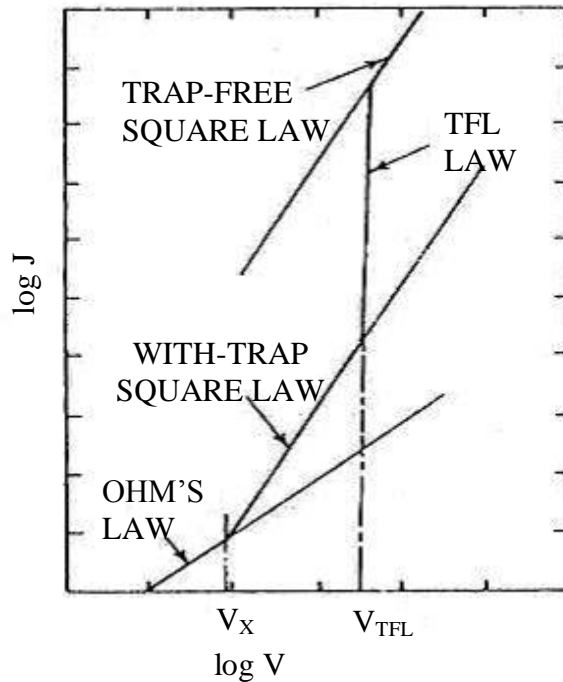
Fig. 2.19: Space charge limited conduction characteristic for an insulator containing shallow traps.

traps, and the others below the Fermi level being the deep traps. During trapping both shallow and deep traps would get filled. The voltage at which all the traps would get completely filled is called the trap filled limit (TFL). Beyond V_{TFL} all the excess

charges would be injected into the conduction band and the current would approach the trap free square law as described in Eq[n] (2.16) [2.41, 2.42].

2.9.4   Thermally activated conduction processes

Electronic conduction in organic, molecular compounds differs in several important ways from the more familiar kind in metals and semiconductors. An important feature of the band system is that electrons are delocalized and spread over the lattice. Some delocalization are naturally expected when an atomic orbital of any atom overlaps appreciably with those of more than one of its neighbors, but delocalization reaches an extreme form in the case of a regular 3 dimensional lattice. The band theory assumes that the electrons are delocalized and can extend over the lattice. When electronic conduction is considered in polymers, band theory is not totally suitable because the atoms are covalently bonded to one another, forming polymeric chains that experience weak intermolecular interactions. But macroscopic conduction will require electron movement, not only along the chain but also from one chain to another.

If two solids are put in contact, the Fermi levels equalize at the interface, the other energy levels moving to accommodate this. In pure insulator the Fermi level bisects the forbidden band. Impurities may introduce allowed levels into the forbidden band, and this moves the Fermi level up and down.

As the temperature is increased the charge carrier concentration increases strongly with temperature. This dominates the temperature dependence of the conductivity, giving it an Arrhenius - like character.

It is difficult to generalize about the temperature dependence of dc conduction whether it is ionic or electronic since so many processes are possible. Ohmic (low field) conduction whether ionic or electronic, gives exponential temperature dependence, given by

$$J = J_0 \exp \frac{-\Delta E}{kT}$$ …………………………………… (2.17)

where J_0 is a constant and ΔE is the activation energy for carrier generation. Now

$$J = Ne\mu$$ …………………………………… (2.18)

Where N is the number of charge carriers, e their charge, and μ their mobility. With extrinsic ionic conduction, it is the mobility i.e. the activated process, *ΔE* being the energy for the ion to hop. With extrinsic electronic conduction, the electrons may move by hopping. However, if the electronic conduction is by excitation into the conduction band, the production of free electrons, n not their mobility, μ is activated. Whatever the Ohmic mechanism, a log J vs. 1/T plot (Arrhenius plot) will usually exhibit increasing linear slopes (activation energies) as T is raised [2.42].

For variable range hopping the electrical conductivity is given by

$$\sigma = \sigma_o \exp - \left(\frac{T_o}{T}\right)^{\frac{1}{d+1}} \dots\dots\dots\dots\dots\dots\dots\dots\dots \quad (2.19)$$

where "d" is the dimensionality of transport, σ is the conductivity, σ_o is the initial value of conductivity, T is the absolute temperature and T_o is the activation energy in terms of temperature.
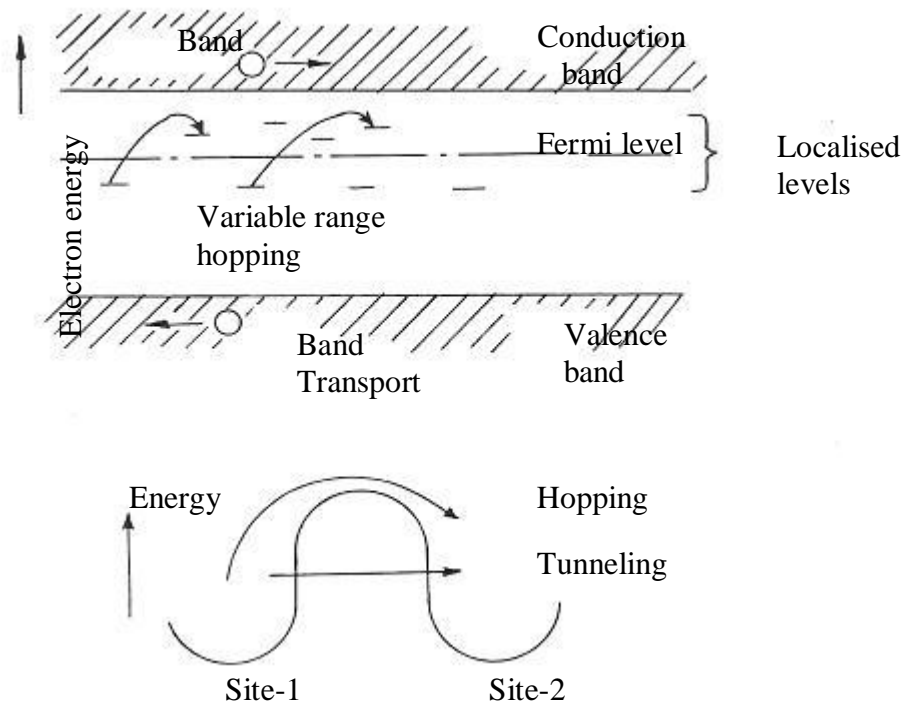
Fig. 2.20: Diagram of electron-transfer mechanisms between adjacent sites separated by a potential-energy barrier.

In bulk material ionic conduction occurs due to the drift of defect under the influence of an applied electric field. The degrees of ionic impurities that may be totally ignored in the context of other properties may have a significant effect on conductivity.

A theoretical expression may be derived for the current density,

$$J = \sin h \, (eaE/2kT)$$ ……………………………. (2.20)

Where E is the electric field, is the distance between neighboring potential wells,

e = charge of electron

References:

[2.1]   Cowie, J. M. G., "Polymers: Chemistry and Physics of Modern Materials", Blackie Academic and Professionals, U K, 2nd Ed. (1991).

[2.2]   Ghosh, P., "Polymer Science and Technology of Plastics and Rubbers", Tata McGraw-Hill Pub. Co. Ltd., New Delhi, 4th Ed., (1996).

[2.3]   Lieberman, M. A. and Lichtenberg A. J., "Principles of Plasma Discharges and Materials Processing", John Wiley and Sons, New York, (1994) .

[2.4]   Grill, A., "Cold Plasma in Materials Fabrication: From Fundamentals to Applications", IEEE Press, New York, (1994),

[2.5]   Bogaerts, A., Wilken, L., Hoffmann, V., Gijbels, R. and Wetzig K., "Comparison of modeling calculations with experimental result for rf glow discharge optical.

[2.6]   Chu, P. K., Chen, J. Y., Wang, L. P. and Huang, N., "Plasma surface modification of biomaterials", Materials Science & Engineering, R: Reports, R36 (5-6), 143-206, (**2002)**.

[2.7]   Yasuda, H., "Plasma Polymerisation", Academic Press, INC: NY, (1985).

[2.8]   Denes, F., "Synthesis and surface modification by macromolecular plasma chemistry", Trends in Polymer Science (Cambridge, United Kingdom)**, 5 (1),** 23-31, (**1997)**.

[2.9]   Bogaerts, A. and Neyts, E., "Gas discharge plasma and their applications", Spectrochimica Acta Part B, **57,** 609-658, (2002) .

[2.10]   Chan, C. M., "Polymer Surface Modification and Characterization", Hanser/Gardner Publications, Inc.: Cincinnatti, OH, (1994).

[2.11]   Chan, C. M., Ko, T. M. and Hiraoka, H., "Polymer surface modification by plasmas and photons", Surface Science Reports, **24** (1/2), 1‐54, (1996).

[2.12] Gibalov, V. I., "Synthesis of ozone in a barrier discharge", Russ. J. Phys. Chem., **68**, 1029-1033, (1994).

[2.13] Wang, X., Zheng, W.T., Tian, H.W., Yu, S.S., Xu, W., Meng, S.H., He, X.D., Han, J.C., Sun, C.Q. and Tay, B.K. "Growth, structural, and magnetic properties of iron nitride thin films deposited by dc magnetron sputtering", Appl. Surf. Sci.*,* **220**, 30-39, (2003).

[2.14] Leonhardt, D., Muratore, C., Walton, S.G., Blackwell, D.D., Fernsler, R.F. and Meger, R.A., "Generation of electron-beam produced plasmas and applications to surface modification", Surf. Coat. Technol., **177-178**, 682-687, (2004).

[2.15] Schlemm, H., Mai, A., Roth, S., Roth, D., Baumgärtner, K.-M. and Muegge, H., "Industrial large scale silicon nitride deposition on photovoltaic cells with linear microwave plasma sources", Surf. Coat. Techno., **174-175**, 208-211, (2003).

[2.16] Yasuda, H., Vossen, J. L., and Kern, W., "Thin Film Processes", Academic Press, New York, (1978).

[2.17] Yasuda, H. and Hirotsu, T., "Critical evaluation of conditions of plasma polymerization", J. Polym. Sci., Polym. Chem. Ed., **16,** 313-317, (1978).

[2.18] Yasuda, H. and Lamaze C. E., "Polymerization in an electrode less glow discharge. III. Organic compounds without olefinic double bond", J. Appl. Polym. Sci., **17,** 1533-1544, (1973).

[2.19] Kinloch, A.J., Adhesion and Adhesives, Science and Technology, Chapman and Hall: New York, 1987.

[2.20] Liston, E.M., Martinu, L., and Wertheimer, M.R., Plasma surface modification of polymers, M. Strobel, C. Lyons and K.L. Mittal, Eds; VSP: The Netherlands, 1994.

[2.21] Yasuda, H., Marsh. H. C., Bumgarner, M. O. and Morosoff, N., "Polymerization of organic compounds in an electrodeless glow discharge. VI. Acetylene with unusual comonomers", J. Appl. Polym. Sci., **19,** 2845-2858, (1975).

[2.22] Davis, E. A. and Mott, N. F., "Conduction in non-crystalline system, Optical absorption and photoconductivity in amorphous semiconductors", Philos. Mag. **22,** 903-922, (1970).

[2.23] Tauc, J., Menth, A. and Wood, D., "Optical and magnetic investigations of the localized states in semiconducting glasses", Phys. Rev. Lett., **25**, 749-752, (1970).

[2.24] Metha,   Akul   "Limitations   and   Deviations   of   Beer-Lambert Law", PharmaXChange.info (2012).

[2.25] Chen C. Ku and Raimond Liepins, "Electrical Properties of Polymers", Hanser Publishers, Munich - Vienna – New York (1987).

[2.26] Yasuda H., "Plasma Polymerization", Academic Press, Inc, New York (1985).

[2.27] Mathai C. J., Saravanan S., Jayalekshmi S., Venkatachalam S., Anantharaman M. R., "Conduction mechanism in plasma polymerized aniline thin films", Mater. Lett, **57**, 2253-2257, (2003).

[2.28] Nagaraj N., Subba Reddy Ch. V., Sharma A. K., Narasimha Rao V. V. R.. J., "DC conduction mechanism in polyvinyl alcohol films doped with potassium thiocyanate", Power Sources, **112**, 326-330, (2002).

[2.29] Sajeev U. S., Mathai, C. J., Saravanan S, Ashokan R, Venkatachalam S., Anantharaman, "On the optical and electrical properties of rf and a.c. plasma polymerized aniline thin films", Bull. Mater. Sci., **29**, No.2 (2006).

[2.30] Sayed W. M. Salem. T. A., "Preparation of polyaniline and studying its electrical conductivity", J. Appl. Polym. Sci., **77**, 1658-1665,(2000).

[2.31] Chowdhury F-U-Z, Bhuiyan A. H., "The dc electrical conduction mechanism of heat-treated plasma-polymerized diphenyl (PPDP) thin films", Indi. J. Phys., **76,** 239-244,(2002).

[2.32] Akther H. and Bhuiyan A. H. "Space charge limited conduction in plasma polymerized N, N, 3, 5 tetramethylaniline thin films", New J. Phys. **7**, 173, (2005).

[2.33] Shah Jalal A.B.M., S. Ahmed, A.H. Bhuiyan and M. Ibrahim, "On the conduction mechanism in plasma-polymerized m-Xylene thin films", Thin Solid Films, **288,** 108-111, (1996).

[2.34] Kumar. S., Nakamura K., Nishiyama S., Ishii S., Noguchi H., Kashiwagi K., Yoshida Y., "Optical and electrical characterization of plasma polymerized pyrrole films", J. Appl. Phys. **93**, 2705-2711, (2003).

[2.35] Silverstein M. S., Visoy-Fisher I., "Plasma polymerized thiophene: molecular structure and electrical properties", Polymer, **43**, 11-20, (2002).

[2.36] John R. K., Kumar D. K., "Structural, electrical and optical studies of plasma polymerized and iodine doped polypyrrole", J. Appl. Polym. Sci., **83**, 1856-1859, (2002).

[2.37] Valaski R., Ayoub S., Micaroni L., Hummelgen I.A., "Influence of thin thickness on charge transport of electrodeposited polypyrrole thin films", Thin Solid Films, **415,** 206-210, (2002).

[2.38] El-Nahass M. M., Abd-El-Rahman K. F., Darwish A. A. A., "Electrical conductivity of 4- tricyanovinyl-N,N-diethylaniline", Physica **B 403**, 219-223, (2008).

[2.39] Bae I.-S., Jung C.-K., Cho S.-J., Song Y.-H., Boo J.-H., "A comprehensive study of plasma polymerized organic thin films on their electrical and optical properties", J. Alloys and Compounds, **449**, 393-396, (2008).

[2.40] Gould R.D. and Lopez M.G., "Poole-Frenkel conductivity prior to electroforming in evaporated Au-SiO$_x$-Au-sandwich structures", Thin Solid Films **342-344,** 94-97, (1999).

[2.41] Bhattacharyya S., Laha A., and Krupanidhi S. B. "Analysis of leakage current conduction phenomenon in thin SrBl$_2$Ta$_2$O$_9$ films grown by excimer laser ablation" J. Appl. Phys. **91**, 4543-4548, (2002).

[2.42] Maisel Leon I, and Glang R., "Hand Book of Thin Film Technology", McGraw Hill Book Company, NY, (1970).

CHAPTER III

MATERIALS and EXPERIMENTAL DETAILS

3.1   Introduction

This chapter describes the experimental details related to thermal, structural, optical and electrical characterizations of plasma polymerized Ortho-methoxyaniline-N,N,3,5-tetramethylaniline (PP(MA-TMA)) composite thin films that include physical properties of Ortho-methoxyaniline and N,N,3,5-tetramethylaniline (monomers), substrate materials, capacitively coupled plasma polymerization set up, film thickness measurement, electrode material and contact electrode deposition technique, electrical measurements. The techniques applied for characterization of PP(OMA-TMA) thin films, such as DTA, TGA, FTIR, for structural, UV-Vis Spectroscopy and electrical measurements are discussed.

3.2   Monomers

Ortho-methoxyaniline (CH_3O-C_6H_4-NH_2) (OMA) in liquid form was used as organic precursor. The monomer Ortho-methoxyaniline is manufactured by BDH Chemicals Ltd., Poole, England and is collected from local market. The chemical structure of the monomer is shown in Fig. 3.1.
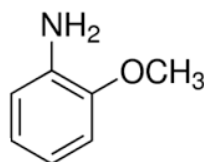
Fig. 3.1: Chemical Structure of Ortho-methoxyaniline

N,N,3,5-tetramethylaniline (CH_3-CH_3-C_6H_3N-CH_3-CH_3) (TMA) was used as a organic precursor (Aldrich-Chemie D-7924, Steinheim, Germany). It is a colored (orange) liquid. TMA contains four methyl groups where two groups are attached to the nitrogen atom. The chemical structure of the monomer is shown in Fig. 3.2.
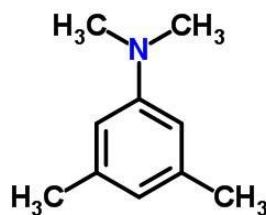
Fig. 3.2: Chemical Structure of N,N,3,5-tetramethylaniline

The physical properties of OMA and TMA are described in Table 3.1.

Table 3.1 Physical properties of Ortho-Methoxyaniline and N,N,3,5-tetramethylaniline

Commercial Name	o-Anisidine	3,5-Xylidine
IUPAC name	2-Methoxyaniline	N,N,3,5-tetramethylaniline
Form	Clear liquid	Clear liquid
Molecular formula	C_7H_9NO	$C_{10}H_{15}N$
Chemical formula	$CH_3O\text{-}C_6H_4\text{-}NH_2$	$CH_3\text{-}CH_3\text{-}C_6H_3N\text{-}CH_3\text{-}CH_3$
Molecular weight	123.15246 g/mol	149.2328 g/mol
Density	1.0923 g/cm^3 at 25 °C	0.913 g/cm^3 at 25 °C
Boiling point	224 °C	226-228 °C

3.3   Procedure of Composite Thin Film Preparation

The composite were prepared with equal concentration mixture ratio of Ortho-methoxyaniline and N,N,3,5-tetramethylaniline monomers.

3.4   Substrate and Its Cleaning Process

A well cleaned substrate is a prerequisite for the preparation of plasma polymerized thin films. Glass slides (dimension: 25.4 mm × 76.2 mm × 1.1 mm) (Sail brand, China) were used as substrates in this research work. Before thin film deposition the substrates were cleaned with acetone and distilled water in an ultrasonic bath. The cleaned glass plates were next rinsed with deionized water and then dried.

3.5   Capacitively Coupled Plasma Polymerization Set-up

Glow discharge plasma polymerization setup has been used enormously in recent years to form various kinds of plasma polymers. Different configuration of polymerization set up varies the properties of plasma polymers.

Fig. 3.3: The plasma polymerization set-up

1	high voltage power supply
2	pirani gage
3	high tension leads
4	gas inlet valve,
5	gauge head
6	monomer injection valve
7	flow meter
8	monomer container
9	Pyrex glass dome
10	metal electrodes
11	electrode stands
12	gasket
13	lower flange
14	bottom flange
15	brass tube
16	valve
17	liquid nitrogen trap
18	rotary pump
19	switch
20	variac

Fig. 3.4: A schematic diagram of the plasma polymerization set-up

The glow discharge plasma polymerization setup used to deposit the PP(OMA-TMA) thin films consists of different components are shown in Fig.3.3 and Fig. 3.4.

Plasma reaction chamber

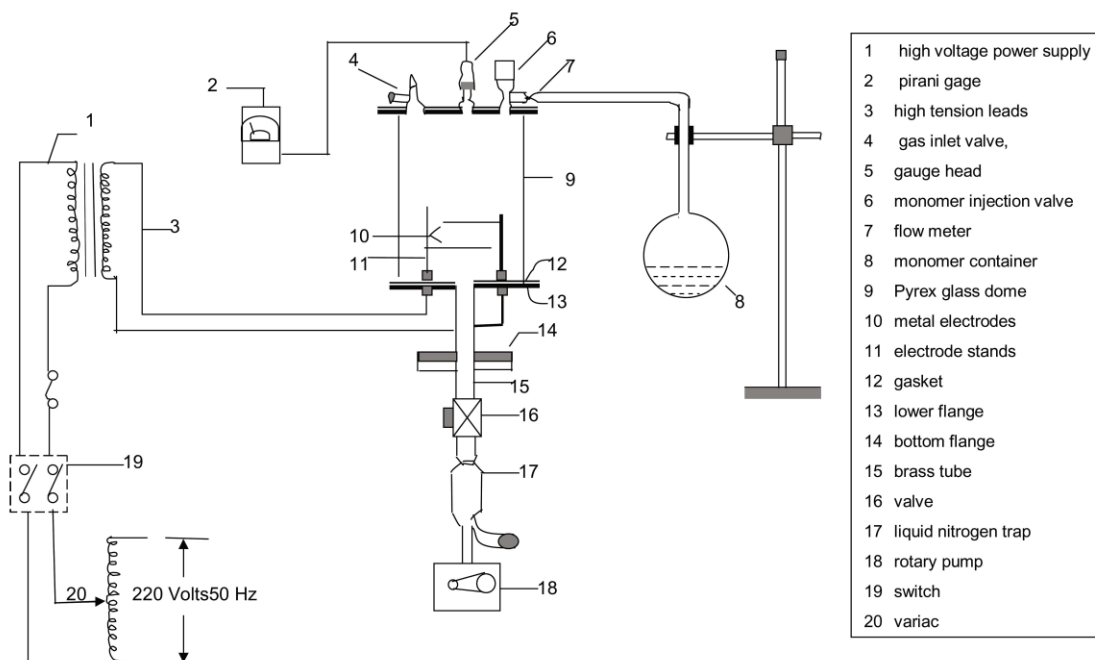The glow discharge reactor is made up of a cylindrical Pyrex glass bell-jar having 0.15 m in inner diameter and 0.18 m in length. The top and bottom edges of the glass bell-jar are covered with two rubber L -shaped (height and base 0.015 m, thickness 0.001 m) gaskets. The cylindrical glass bell jar was placed on the lower flange. The lower flange is well fitted with the diffusion pump by an 'I' joint. The upper flange is placed on the top edge of the bell-jar. The flange is made up of brass having 0.01 m in thickness and 0.25 m in diameter. On the upper flange a laybold pressure gauge head, Edwards high vacuum gas inlet valve and a monomer injection valve are fitted. In the lower flange two highly insulated high voltage feed-through are attached using screwed copper connectors of 0.01m high and 0.004 m in diameter via Teflon™ insulation.

Some important parts of plasma polymerization set up are:

1. High voltage power supply	11. Electrode stands
2. Pirani gage	12. Gasket
3. High tension leads	13. Lower flange
4. Gas inlet valve	14. Bottom flange
5. Gauge head	15. Brass tube
6. Monomer injection valve	16. Valve
7. Flow meter	17. Liquid nitrogen trap
8. Monomer container	18. Rotary pump
9. Pyrex glass dome	19. Switch
10. Metal electrodes	20. Variac

3. 6   Deposition of Plasma Polymerized Thin Film

Glow discharges are produced by an applied static or oscillating electric field where energy is transferred to free electrons in vacuum. Inelastic collisions of the energetic free electrons with the gas molecules generate free radicals, ions, and species in electronically excited states. This process also generates more free electrons, which is necessary for a self-sustaining glow.

The important feature of glow discharge plasma considered for the purpose of plasma polymerization is the non-equilibrium state of the overall system. In the plasmas, most of the negative charges are electrons and most of the positive charges are ions. Due to large mass difference between electrons and ions, the electrons are very mobile as

compared to the nearly stationary positive ions and carry most of the current. Energetic electrons as well as ions, free radicals, and vacuum ultraviolet light can possess energies well in excess of the energy sufficient to break the bonds of typical organic monomer molecules which range from approximately 3 to 10 eV. Some typical energy of plasma species available in glow discharge as well as bond energies encountered at pressure of approximately 10^{-2} Torr.

Fig. 3.5: Glow discharge plasma during deposition

The chamber of the glow discharge reactor is evacuated to about 0.01 Torr. A high-tension transformer along with a variac is connected to the feed-through attached to the lower flange. While increasing the applied voltage, the plasma is produced across the electrodes at around 10^{-1} to 10^{-2} Torr chamber pressure. After finding the desired plasma glow in the reactor the monomer vapor is injected downstream to the primary air glow plasma for some time. Incorporation of monomer vapor changed the usual color of plasma which is shown in Fig. 3.5. The deposition time was varied from 20-80 minutes to get the PP(OMA-TMA) thin films of different thicknesses. The optimized conditions of thin film formation for the present study are:

Table 3.2: The optimum plasma polymerization condition for PP(OMA-TMA)

Separation between two electrodes	4 cm
Deposition power	40 W
Position of the substrate	Lower electrode
Deposition time	20 to 80 min
Pressure in the reactor	10^{-1} to 10^{-2} Torr

3.7   Contact Electrodes for Electrical Measurements

3.7.1   Electrode material

Aluminium (*Al*) (purity of 4N British Chemical Standard) was used for electrode deposition. *Al* has been reported to have good adhesion with glass slides [3.1]. *Al* film has advantage of easy self-healing burn out of flaws in sandwich structure [3.2].

Fig. 3.6: The Edward vacuum coating unit E306A.

3.7.2   Electrode deposition

Electrodes were deposited using an Edward coating unit E-306A (Edward, UK). The system was evacuated by an oil diffusion pump backed by an oil rotary pump. The chamber could be evacuated to a pressure less than 10^{-5} Torr.
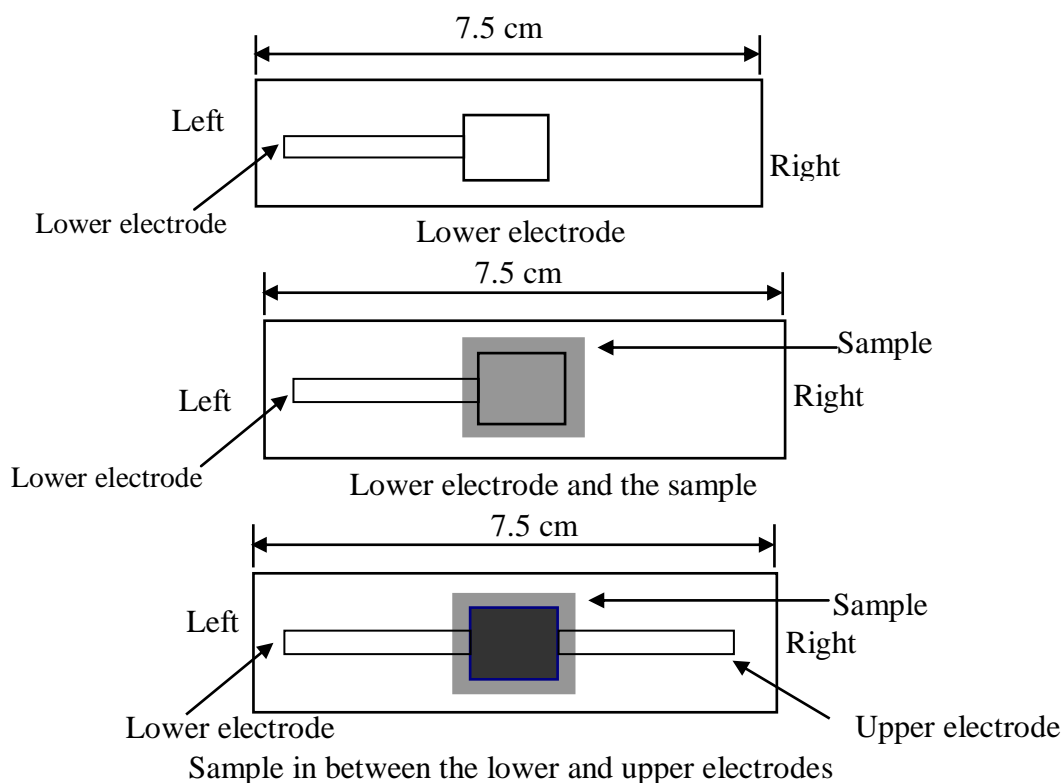
Fig. 3.7: The electrode sample arrangement for the electrical measurement.

The glass substrates were masked with 0.08 m × 0.08 m × 0.001 m engraved brass sheet for the electrode deposition. The electrode assembly used in the study is shown in Fig. 3.7. The glass substrates with mask were supported by a metal rod 0.1 m above the tungsten filament. For the electrode deposition *Al* was kept on the tungsten filament. The filament was heated by low-tension power supply of the coating unit. The low-tension power supply was able to produce 100 A current at a potential drop of 10 V. During evacuation of the chamber by diffusion pump, the diffusion unit was cooled by the flow of chilled water and its outlet temperature was not allowed to rise above 305K. When the Penning gauge reads about 10^{-5} Torr, the *Al* on tungsten filament was heated by low-tension power supply until it was melted.

The *Al* was evaporated to deposit lower electrode onto the glass slide. *Al* coated glass substrates were taken out from the vacuum coating unit and were placed on the middle of the lower electrode of the plasma deposition chamber for PP(OMA-TMA) thin film deposition under optimum condition. The top *Al* electrode was also prepared on the PP(OMA-TMA) film as described above.

3.8   Measurement of Thickness of the Thin Films

Thickness is the single most significant film parameter. It may be measured either by in-situ monitoring of the rate of deposition, or after the film is taken out of deposition chamber. Techniques of the first type often called as monitor method generally allow both monitoring and controlling of the deposition rate and film thickness. Other techniques are also used for thickness measurement. Any physical quantity related to film thickness can in principle be used to measure the film thickness. It may be measured either by several methods with varying degrees of accuracy. The methods are chosen on the basis of their convenience, simplicity and reliability. Since the film thicknesses are generally of the order of a wavelength of light, various types of optical interference phenomena have been found to be most useful for measurement of film thicknesses.

Several of the common methods are:
 i) Multiple-Beam Interferometry during Evaporation, ii) Michelson interferometry
iii) Multiple-Beam Interferometry, (Tolansky Fizeau fringes method, Fringes of equal chromatic order.)
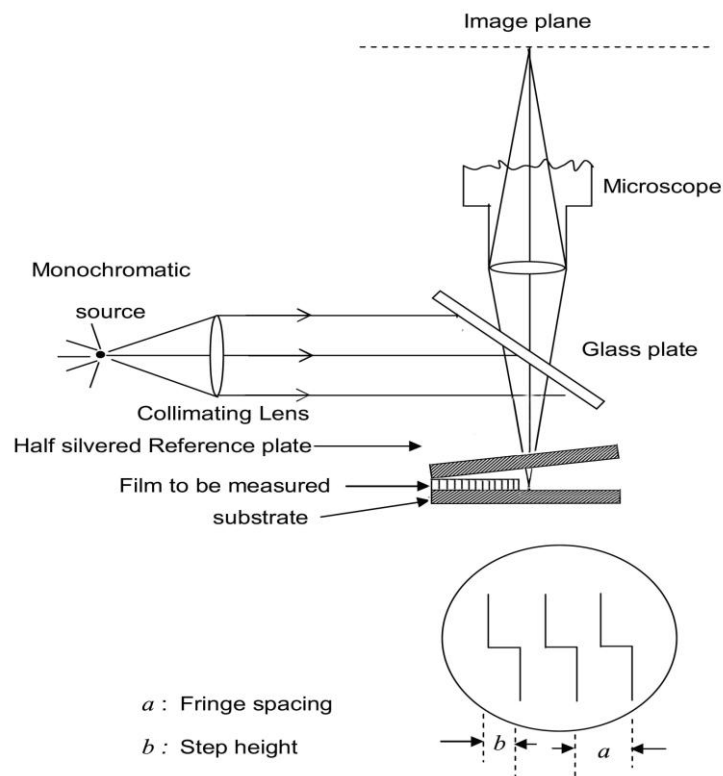

Fig. 3.8: Interferometer arrangement for producing reflection Fizeau fringes of equal thickness.

Multiple-Beam Interferometry technique was employed for the measurement of thickness of the PP(OMA-TMA) thin films. This technique is described below.

This method utilizes the resulting interference effects when two silvered surfaces are brought close together and are subjected to optical radiation. This interference technique, which is of great value in studying surface topology in general, may be applied simply and directly to film thickness determination. When a wedge of small angle is formed between unsilvered glass plates, which are illuminated by monochromatic light, broad fringes are seen arising from interference between the light beams reflected from the glass on the two sides of the air wedge.

At points along the wedge where the path difference between these two beams are an integral and odd number of wavelengths, bright and dark fringes occur respectively. If the glass surfaces of the plates are coated with highly reflecting layers, one of which is partially transparent, then the reflected fringe system consists of very fine dark lines against a bright background. A schematic diagram of the multiple-beam interferometer along with a typical pattern of Fizeau fringes from a film step is shown in Figure. As shown in this figure, the film whose thickness is to be measured is over coated with a silver layer to give a good reflecting surface and a half-silvered microscope slide is laid on top of the film whose thickness is to be determined. A wedge is formed by the two microscope slides and light multiply reflected between the two silvered surfaces forms an interference pattern with a discontinuity at the film edge as shown in Fig. 3.8. The thickness of the film "*d*" can then be determined by the relation,

$$d = \frac{\lambda}{2}\frac{b}{a} \qquad \qquad \ldots \qquad \ldots \qquad \ldots \qquad (3.1)$$

Where, λ is the wavelength and *b/a* is the fractional discontinuity identified in the figure. In general, the sodium light is used, for which λ = 5893 Å. In conclusion, it might be mentioned that the Tolansky method of film-thickness measurement in which a traveling microscope measures the step height and width of the Fizeau fringes that are formed due to the interference of light reflected from the glass and the thin film surfaces having path difference an integral or odd number multiple of wavelength is the most widely used and in many respects also the most accurate and satisfactory one . For film thickness measurement separate glass slide has been used in addition to the sample

substrates. Teflon tape was used to cover 50% area of the cleaned glass, which was not exposed to plasma environment during plasma polymerization. After deposition, the Teflon tape was carefully removed from the glass slide. The step generated on the surface of the glass slide was used to measure the film thickness.

3.9   Field Emission Scanning Electron Microscopy

The surface morphology of the PP(OMA-TMA) thin films have been investigated by the field emission scanning electron microscopy (FESEM) [JEOL JSM 7600F, Japan] with an operating voltage of 5 kV and with two magnification ($\times$ 50,000 and $\times$100,000). The energy dispersive analysis of X-rays (EDAX) which is connected to the microscope also performed for the elemental analysis of the samples. Small pieces (1 cm$\times$ 1 cm) of glass were cut at first for PP(OMA-TMA) thin film deposition. Before thin film deposition the substrates were cleaned with acetone and distilled water. Then PP(OMA-TMA) thin films were deposited on these cleaned substrates. Prior to FESEM recording the film surface was coated with a thin layer of platinum by sputtering to avoid the charging effect. Micrographs were taken at varying points for different magnifications. Fig. 3.9 shows the different parts of the Scanning electron microscope used in the study of the surface morphology.

Fig. 3.9: Field emission scanning electron microscope, JEOL JSM 7600F

The data generated by EDAX consist of spectra showing peaks corresponding to the elements making up the true composition of the sample being analyzed. In a multi-

technique approach EDAX becomes very powerful, particularly in contamination investigations. EDAX of the deposited and heat treated PP(OMA-TMA) thin films were performed by using an energy dispersive X-ray detector attached to the FESEM instrument. EDAX spectra were recorded at various points of the PP(OMA-TMA) films to identify the percentage of carbon, nitrogen and oxygen present in these films.

3.10   Fourier Transform Infrared Spectroscopy

Fourier transform infrared (FTIR) spectra of PP(OMA-TMA) were recorded at room temperature by using a double beam IR spectrophotometer (SHIMADZU, FTIR-8900 spectrophotometer, JAPAN) in the wave-number range of 400-4000 cm^{-1}. The FTIR spectrum of the monomer OMA-TMA was obtained by putting the liquid monomer in a potassium bromide (KBr) measuring cell. PP(OMA-TMA) powder was collected from the PP(OMA-TMA) deposited substrates and then pellets of PP(OMA-TMA) powder mixed with KBr were prepared for recording the FTIR spectra of PP(OMA-TMA) sample. The FTIR spectra of the OMA-TMA and the PP(OMA-TMA) were recorded in transmittance (%) mode.

3.11   Thermal Analyses

Thermal analysis comprises a group of techniques in which a physical property of a substance is measured as a function of temperature, while the substance is subjected to a controlled temperature programme. In differential thermal analysis, the temperature differences that develops between a sample and an inert reference material is measured, when both are subjected to identical heat treatments. Melting and degradation temperatures of the neat PP(OMA-TMA) samples were monitored by a DTA and thermogravimetric analyzer (TGA) [Seiko-Ex-STAR-6300, Japan]. The measurements using DTA and TGA were carried out from room temperature (300 K) to 800 K at a heating rate of 20K/min under nitrogen gas flow. While the DTA traces give the melting and degradation temperatures as determined from the exotherm versus temperature curves, the TGA runs exhibit the weight-loss of the sample with temperature.

3.12   Ultraviolet Visible Spectroscopy

The optical properties of the PP(OMA-TMA) thin films deposited on glass substrates having a dimension of (0.018 m $\times$0.018 m $\times$0.012 m) were studied by UV-vis spectroscopic measurements. The UV-vis absorption spectra of PP(OMA-TMA) thin

films were recorded using a dual beam UV-vis spectrophotometer (SHIMADZU, UV-1601) in the wavelength range of 200-800 nm (Fig. 3.10).

Fig. 3.10: The UV- Visible spectrometer Shimadzu UV-1601

Different PP(OMA-TMA) samples were heat treated at 473 and 573 K in air for one hour in a carbolite furnace mentioned earlier. A similar blank glass slide was used as the reference during the optical absorption measurement of PP(OMA-TMA) thin films. Samples of different thicknesses were used for UV vis spectroscopic study.

3.13   Direct Current Electrical Measurement

Suitable electrical contacts were made with the *Al* electrode by fine conducting copper wire using silver paste. Now the samples are ready for DC electrical measurements. The electrical measurements were carried out in the PP(OMA-TMA) films by loading the samples in a cylindrical metal holder. The measurements were carried out under dynamic vacuum of about 1.33 Pa. The current flowing through the films was measured by using a high impedance KEITHLEY 6517B electrometer. DC bias voltage was applied by an Agilent 6545A stabilized DC power supply. The DC measurements were carried out at different constant temperatures (298, 323, 348, 373 and 398 K). The sample chamber as well as the samples was heated by a heating coil wrapped around the specimen chamber. A Chromel-Alumel thermocouple mounted on the sample holder, with the fused end in contact with the PP(OMA-TMA) thin film, permitted temperature measurements using a 197A digital microvoltmeter (DMV). The block

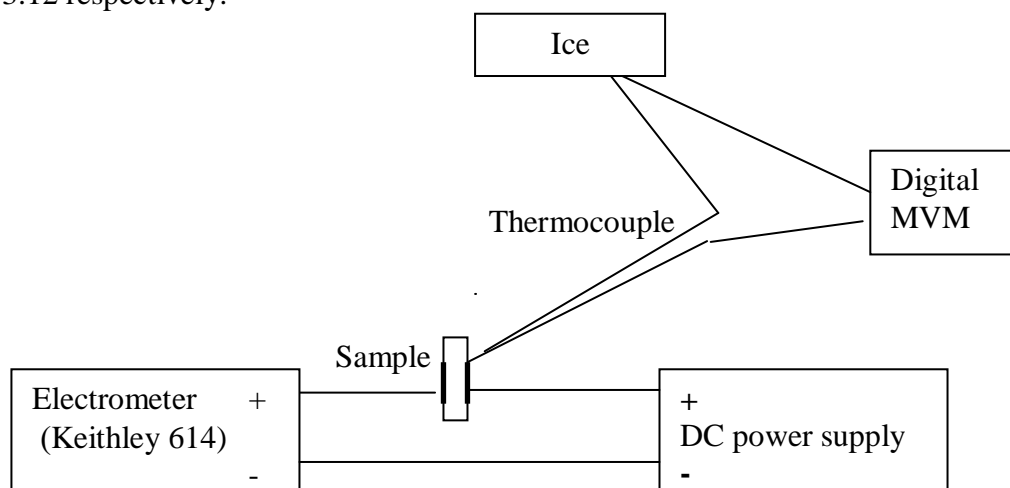diagram for DC measurements and DC measurement set up are shown in Fig. 3.11 and Fig. 3.12 respectively.

Fig. 3.11: A schematic circuit diagram for DC measurements

Fig. 3.12: Arrangement of DC electrical measurement set-up.

References:

[3.1]   Lamb, D. R., "Electrical Conduction Mechanisms in Thin Insulating Films", Methuen and Co. Ltd., London, (1967).

[3.2]   Shah Jalal, A. B. M., Ahmed, S., Bhuiyan, A. H. and Ibrahim, M., "UV-VIS Absorption Spectroscopic Studies of Plasma-Polymerized M-Xylene Thin-Films", Thin Solid Films, **288**, 108-111, (1996).

[3.3]   Phadke, S. D., Sathianandan, K. and Karekar, R. N., "Electrical conduction in polyferrocene thin films", Thin Solid Films, **51,** 9-11, (1978).

[3.4]   Gould, R. D. and Shafai, T. S., "Conduction in lead phthalocyanine films with aluminim electrodes", Thin Solid Films, 373 (1-2), 89-93, (2000).

CHAPTER IV

RESULTS AND DISCUSSION

4.1   Introduction

Plasma polymerized thin films have received much attention of the researchers and scientists for their usefulness in photovoltaic energy converters, photodiodes, optoelectronics, sensors, dielectrics, etc [4.1-4.3]. For these kinds of applications further investigations of the optical and electrical properties of plasma polymerized thin films are needed. In view to this the optical and electrical properties of the PP(OMA-TMA) thin films were studied and the allowed direct and indirect optical transition energy gaps and dc conduction mechanism have been evaluated from the UV-Visible spectroscopic and dc electrical studies respectively and are discussed in this chapter. The structural and thermal analyses of the PP(OMA-TMA) thin films are also discussed in short in this chapter which helps to correlate the optical and electrical results.

4.2   Field Emission Surface Morphology

The field emission scanning electron micrographs (FESEM) of PP(OMA-TMA) thin films were recorded at different point at different magnifications (50000×, 100000×) at accelerating voltage of 10 kV which are shown in Fig. 4.1. From the micrographs it can easily be visualized that the surface of the PP(OMA-TMA) thin films is uniform, flawless, pinhole and fracture free and no significant change is observed.

EDAX spectrum of PP(OMA-TMA) was recorded by the EDAX setup connected with the SEM and is presented in Fig. 4.2. The observation indicates the presence of carbon, nitrogen and oxygen in the PP(OMA-TMA) thin films which is shown in table 4.1.

Table 4.1: Composition of elements in PP(OMA-TMA) thin films

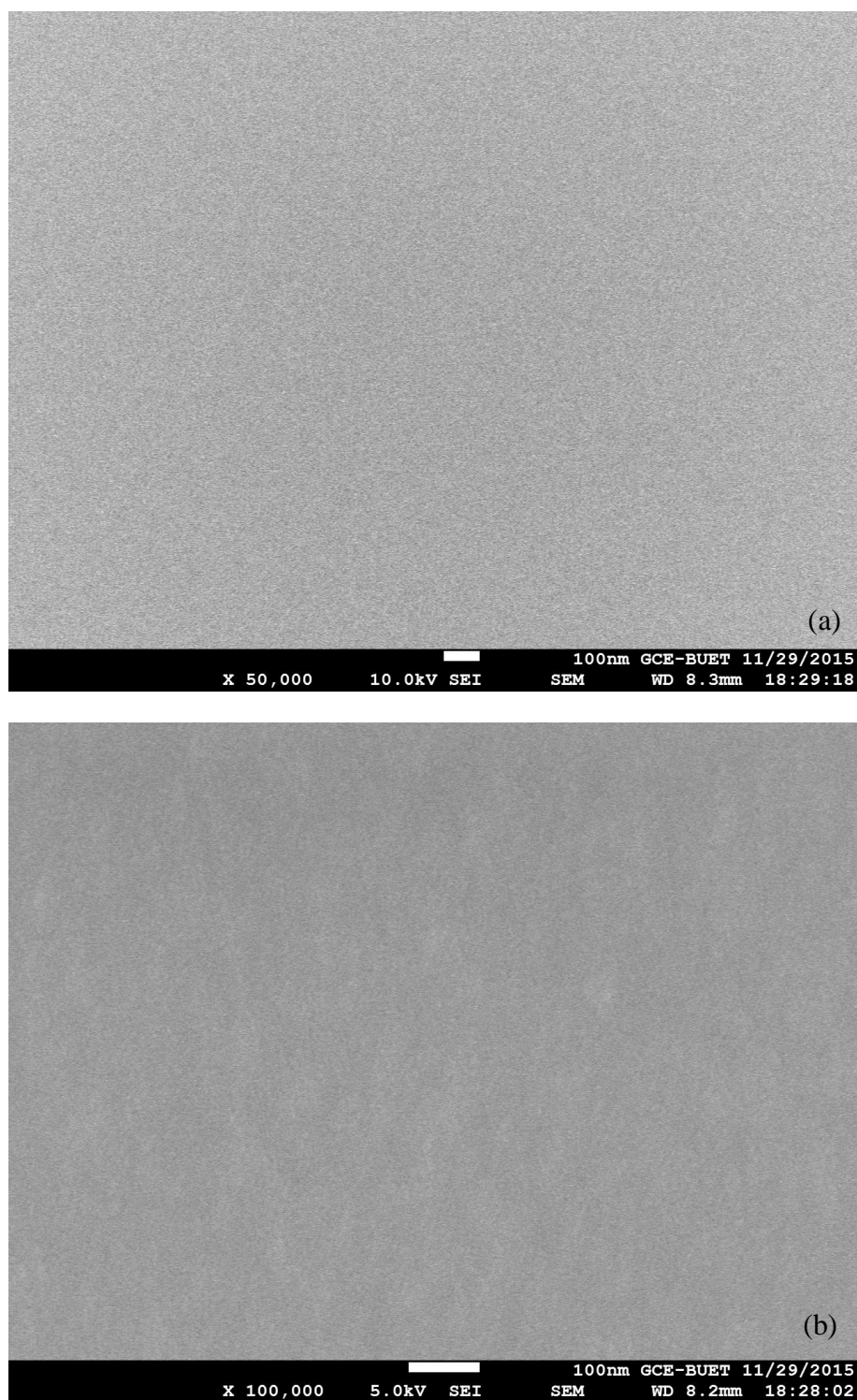| Element	Mass%	Atom%
C	47.22	53.56
N	12.26	11.92
O	40.53	34.52
Total	100.00	100.00

Fig. 4.1: FESEM micrographs of PP(OMA-TMA) thin film (a) ×50K and (b) ×100K
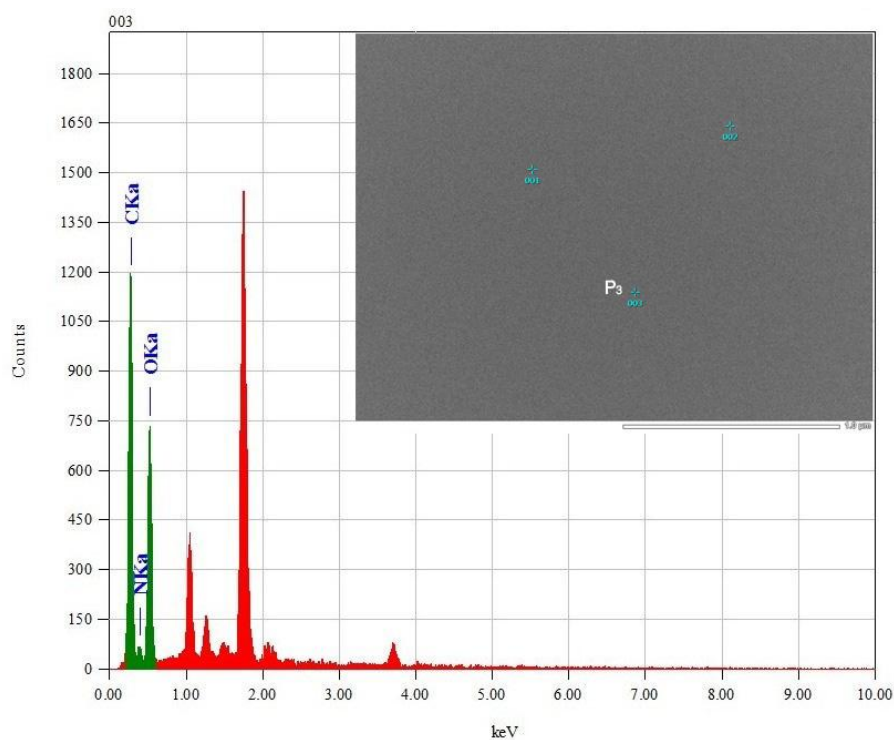
Fig. 4.2: EDAX spectra of PP(OMA-TMA) thin film

From the results it is shown that two strong peaks corresponding to carbon and oxygen are observed in the spectrum of PP(OMA-TMA) thin films. It is clear that carbon has the maximum percentage and the presence of nitrogen follows a good ratio as we can predict from both monomers. The oxygen in the polymer composite is due to the incorporation of surrounding oxygen when samples were taken out side from the reactor chamber. From the EDAX result it is observed that hydrogen cannot be detected.

4.3   Infrared Spectroscopy

The FTIR spectra of the monomers OMA, TMA and PP(OMA-TMA) are shown in Fig. 4.3. It is seen from these spectra that there are structural changes due to plasma polymerization and the structure of the PP(OMA-TMA) thin films deviates to some extent from those of the structures of monomers. It is seen from the FTIR spectrum of the PP(OMA-TMA) thin films that the intensity of the absorption bands decreased significantly compared to those of the monomer spectra. This is an indication of monomer fragmentation during plasma polymerization.

In the spectrum of OMA, bands appeared at 3373 and 3454 cm^{-1} indicate the presence of N-H stretching vibration. The multiple broad peaks confirm ammonium ions in the

structure. The observed peaks at 3001 and 3199 cm^{-1} may be due to aromatic C-H stretching and peak at 2932 cm^{-1} indicates alkyl C-H stretching vibration. The absorption peak observed at 2835 cm^{-1} may be due to the aliphatic -O-CH$_3$ attached to aniline.

The absorption band at 1614 cm^{-1} is observed due to N-H bending. Absorption peak at 1504 cm^{-1} indicates aromatic C=C stretching vibration. Several sharp peaks between 1340 and1460 cm^{-1} are due to C-H bending. The absorption peaks at 1224 and 1275 cm^{-1} corresponds to the C-H twisting and peaks at 1140 and 1182 cm^{-1} corresponds to the C-N stretching. Peaks at 1074, 1045, 1024 cm^{-1} indicates C-O stretching vibration. Bands at 910 and 842 cm^{-1} are observed due to C-H rocking. The band found in 1861-2063 cm^{-1} represents 1, 2-disubstituttion (ortho) in the benzene ring. The strong absorption peak at 740 cm^{-1} confirms ortho and di-substitution in the benzene ring.
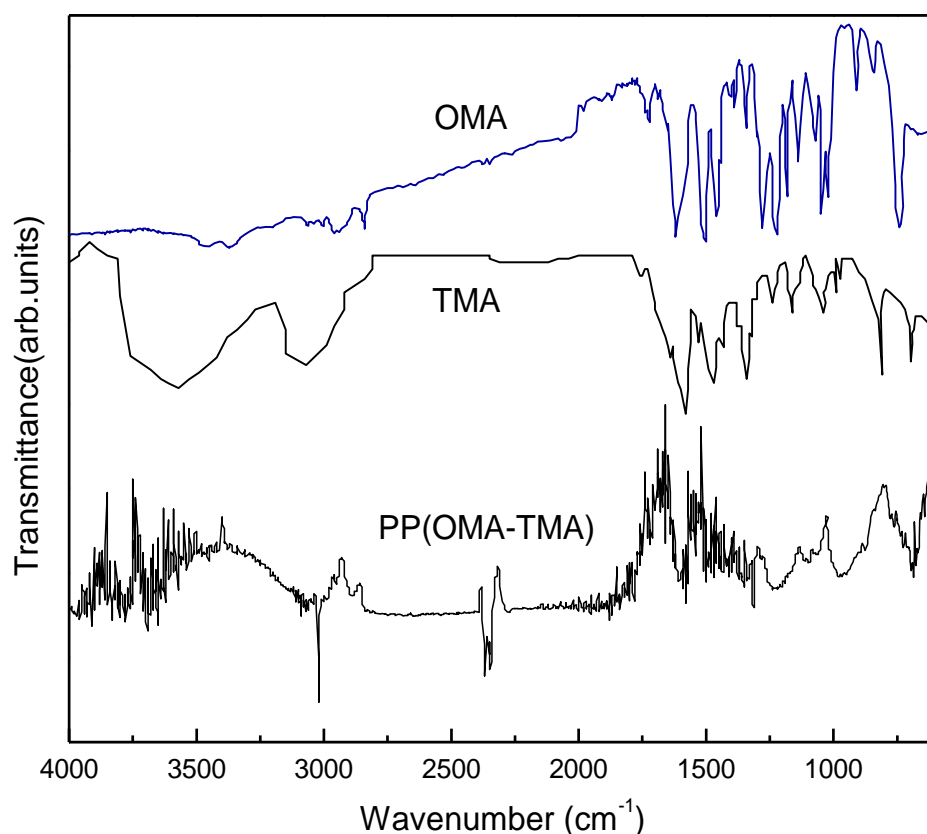

Fig. 4.3: The FTIR spectra of OMA, TMA and PP(OMA-TMA) (Curves are linearly shifted for convenience)

In the spectrum of TMA, the asymmetric N-H stretching band at 3475 cm^{-1} and symmetric N-H stretching band at 3340 cm^{-1}. Relatively strong band at 2935 and 2793 cm^{-1} correspond to the C-H stretching vibrations. The wide band at 1680-1645 cm^{-1} and the absorption peaks at 1484 and 1595 cm^{-1} may be attributable to C=C in aromatic ring stretching vibration of benzenoid and quinoid rings, respectively. Bands at 1351 and 1307 cm^{-1} are observed due to conjugation of the electron pair of the nitrogen atom with the ring imparting double bond character to the C-N bond and a lower frequency band at 1223-1030 cm^{-1} may be due to aliphatic C-N stretching. The band character of tetra substituted benzene is present between 814-776 cm^{-1} in the spectrum.

In the spectrum PP(OMA-TMA) the absorption band at 3382 cm^{-1} may arise due to N-H stretching vibration, which is similar to that in OMA and TMA. An absorption band corresponding to aromatic (sp^2) =C-H vibration is seen at 3020. A band observed at 2924 cm^{-1} corresponds to C-H stretching. An absorption band corresponding to aliphatic -O-CH$_3$ vibration is observed at 2854 cm^{-1}.

Table 4.2: Assignments of FTIR absorption bands for OMA, TMA and PP(OMA-TMA)

Assignments	Wavenumber (cm^{-1})		
	OMA [4.4]	TMA [4.5]	PP(OMA-TMA)
N-H stretching vibration	3373, 3454	3475, 3340	3382
Aromatic (sp^2) =C-H	3199, 3001	-	3020
Alkyl (sp^3) C-H stretching	2932	2935, 2793	2924
Aliphatic -O-CH$_3$ vibration	2835	-	2854
CO$_2$ in the atmosphere	2260	-	2214
1,2-Disubstituttion (ortho) in benzene ring	2063, 1976, 1909, 1861	-	1886
N-H bending	1614	-	1610
C=C stretching	1504	1680-1645	1580
C-H bending	1460, 1404, 1384, 1340	-	-
C-H twisting	1224, 1275	1226, 1017	1307, 1290
C-N stretch	1182, 1140	1351, 1307, 1223-1030	1226, 1095
C-O stretch	1074, 1045, 1024	-	973
C-H rocking intense	910, 842	-	-
Tetra-substituted benzene	-	814-776	-

Carbon dioxide in the atmosphere may also result in an absorption which is found at wavenumber 2260 cm^{-1} in monomer and at 2214 cm^{-1} in PP(OMA-TMA). There is an absorption peak at 1610 cm^{-1} like monomer OMA for N-H bending. The observed absorption peaks at 1580, 1563 and 1502 cm^{-1} may be assigned to C=C stretching [4.6]. Broad band at 1307 and 1290 cm^{-1} indicates the presence of C-H twisting. C-N stretching vibration arises at 1135, 1081 and 1026 cm^{-1}. 1100-973 cm^{-1} band may be assigned to C-O stretching. It is found that the PP(OMA-TMA) thin films deposited by plasma polymerization technique have some absorption bands of the monomers and some are absent.

4.4 Thermal analyses

DTA and TGA traces of the PP(OMA-TMA) thin films taken in the temperature range of 298-800 K at a scan rate of 20 K/min in nitrogen atmosphere are shown in Fig. 4.4. DTA thermogram shows an exotherm, which reaches a maximum at around 680 K and then stable with increasing the temperature. The corresponding TGA trace of PP(OMA-TMA) has been taken from 298-800 K and shows different stages of thermal decomposition, which can be divided in to three regions A, B and C as indicated in Fig. 4.4.
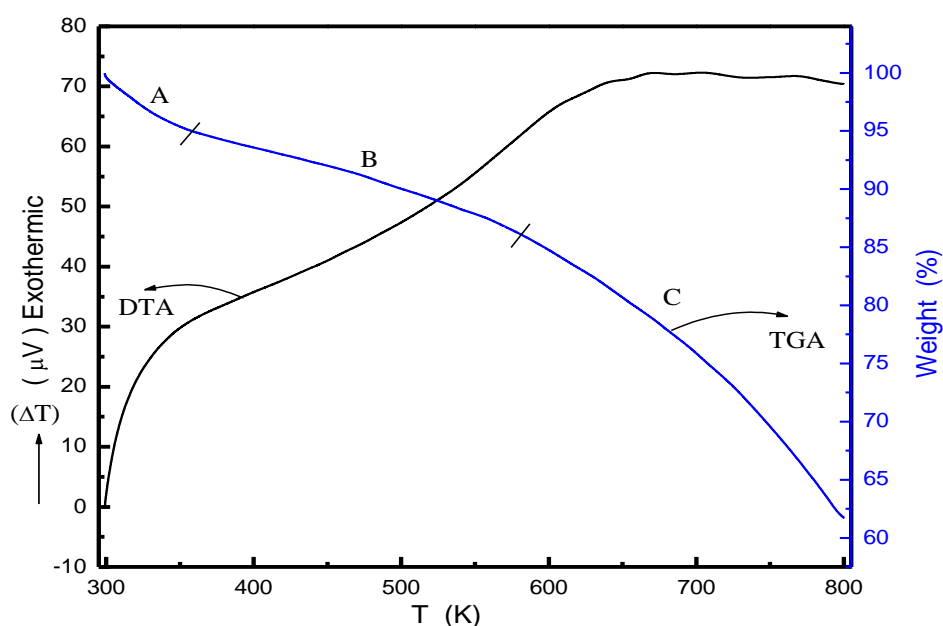

Fig. 4.4: DTA and TGA thermograms of PP(OMA-TMA) thin films.

Every region may be associated with a different rate of weight loss. The weight losses in A, B and C regions are about 5%, 9% and 24% respectively. In the first region A, the weight loss up to 350 K may be related to the removal of water content, which is not necessarily associated with any change in the structure. The 9% of weight loss up to 575 K in the B region may be attributed to the loss of non-constitutional/ adsorbed water/ unreacted monomer which might settled on PP(OMA-TMA) films surface and or due to evolution of hydrogen and low molecular mass hydrocarbons. And the 24% of weight loss in the C region, may be caused by the thermal decomposition of the PP(OMA-TMA) structure and expulsion of higher molecular mass hydrocarbons, oxygen containing compounds, etc. Thus, it can be attributed that PP(OMA-TMA) films are thermally stable up to about 575 K.

4.5   Ultraviolet-visible Spectroscopic Analyses

Fig: 4.5 presents the room temperature UV-Vis absorption spectra for PP(OMA-TMA)
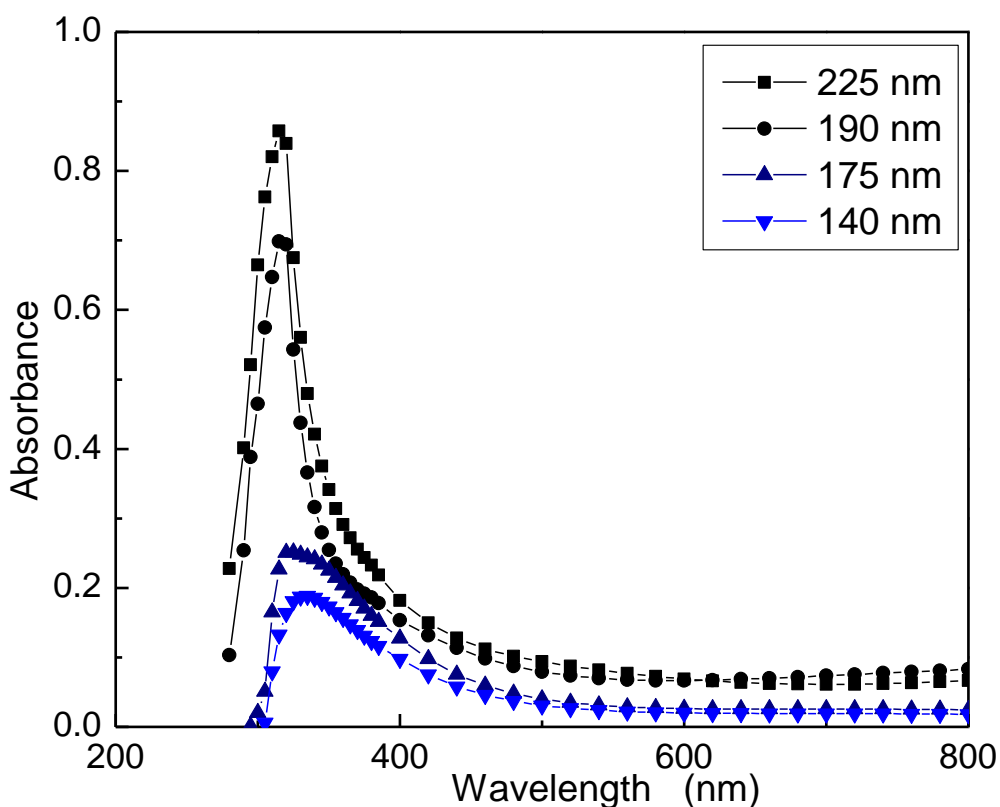

Fig. 4.5: Variation of absorbance with wavelength (λ) for PP(OMA-TMA) thin films of different thicknesses.

thin films of different thicknesses. It is observed that there is a sharp rise in absorbance in the low wavelength region, reaches a maximum, and then absorbance rapidly decreases up to about 400 nm for all the PP(OMA-TMA) thin films. Above 400 nm, absorbance decreases slowly.

The absorbance increases with increasing thickness of the PP(OMA-TMA) thin films. The maximum absorbance wavelengths (λ_{max}) and maximum absorbance values corresponding to PP(OMA-TMA) thin films of different thicknesses are recorded in Table 4.3. The λ_{max} does not vary much and maximum absorbance increases as thickness increases as scattering increasing with thickness.

The absorption coefficient, α is calculated from the measured absorbance data of Fig. 4.5 for different wavelengths corresponding to different photon energies at room temperature by Eq^n 2.5 (chapter II)

Table 4.3: Wavelength corresponding to maximum absorbance (λ_{max}) and maximum absorbance of PP(OMA-TMA) thin films of different thicknesses

Film thickness, d (nm)	Wavelength at maximum absorbance, λ_{max} (nm)	Maximum absorbance
140	333	0.18
175	326	0.25
190	316	0.69
225	318	0.84

The spectral dependence of α on photon energy, hν, for all the deposited samples is presented in Fig. 4.6. The dependence of α on $h\nu$ helps to know the band structure and the type of transition of electrons. The absorption edge starts increasing around 2.25 eV and there is a rapid rise in α from 2.80 eV. It is observed that in the low energy region the curves are non-linear and the edges have an exponential fall for values of α below about 3×10^4 cm^{-1} for all the composite thin films. It is clear from Fig. 4.6 that the curves have different slopes indicating the presence of different optical transitions in the PP(OMA-TMA) thin films. The different optical transition can be determined using the Tauc relation Eq^n 2.8 (chapter II).
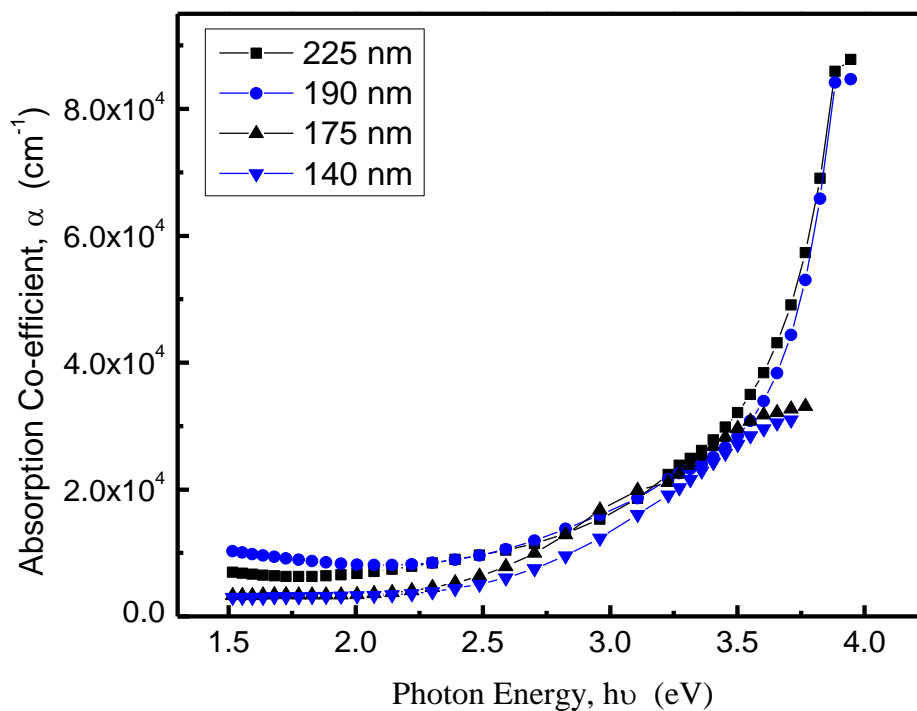
Fig. 4.6: Plot of absorption co-efficient, α, as a function of photon energy, hν, for PP(OMA-TMA) thin films of different thicknesses.
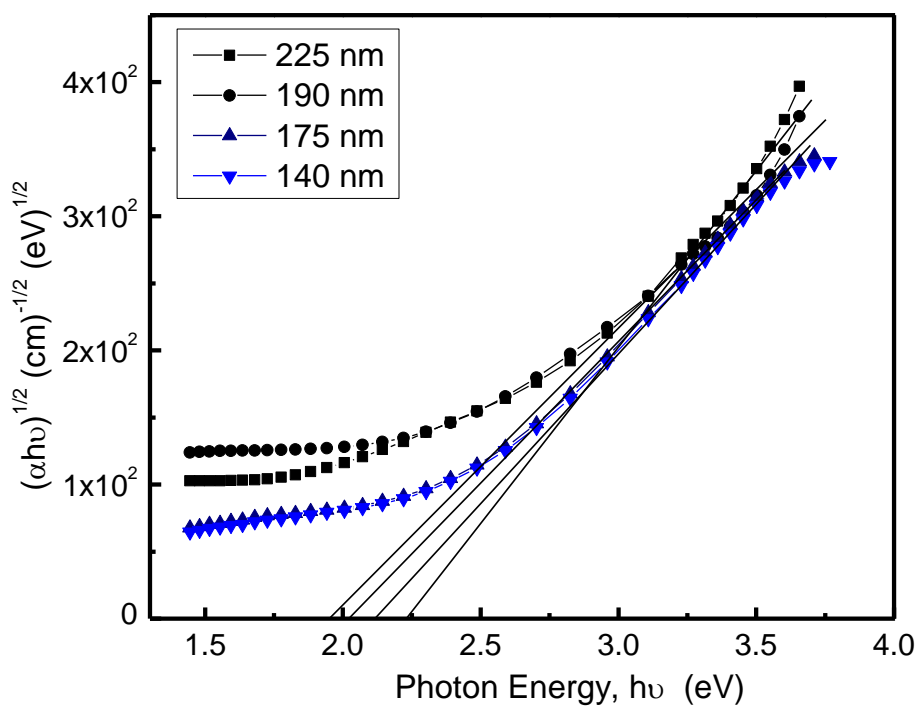

Fig. 4.7: $(\alpha h\nu)^{1/2}$ vs. hν curves for PP(OMA-TMA) thin films of different thicknesses.

The indirect transition energy gap (E_{gi}) can be obtained by plotting $(\alpha h\nu)^{1/2}$ versus $h\nu$ curve and then extrapolating the linear portion of the curve to $(\alpha h\nu)^{1/2} = 0$. Also from the plots of $(\alpha h\nu)^2$ versus $h\nu$, direct transition energy gap (E_{gd}) can be determined from the intercept of the linear part of the curve extrapolated to zero α in the photon energy axis [4.7].

Table 4.4: Direct and indirect band gaps of PP(OMA-TMA) thin films

Thickness d (nm)	Direct Band Gap E_{gd} (eV)	Indirect Band Gap E_{gi} (eV)
225	3.73	2.23
190	3.66	1.95
175	3.20	2.02
140	3.13	2.12

$(\alpha h\nu)^{1/2}$ as a function of $h\nu$ is plotted in Fig. 4.7, to obtain E_{gi} of the PP(OMA-TMA) thin films. In Fig. 4.8, $(\alpha h\nu)^2$ as a function of $h\nu$ is plotted to obtain the allowed direct transition energy gap of the PP(OMA-TMA) thin films. The values of the E_{gd} and E_{gi} for PP(OMA-TMA) thin films determined form Fig. 4.7 and Fig. 4.8 are recorded in Table 4.4.
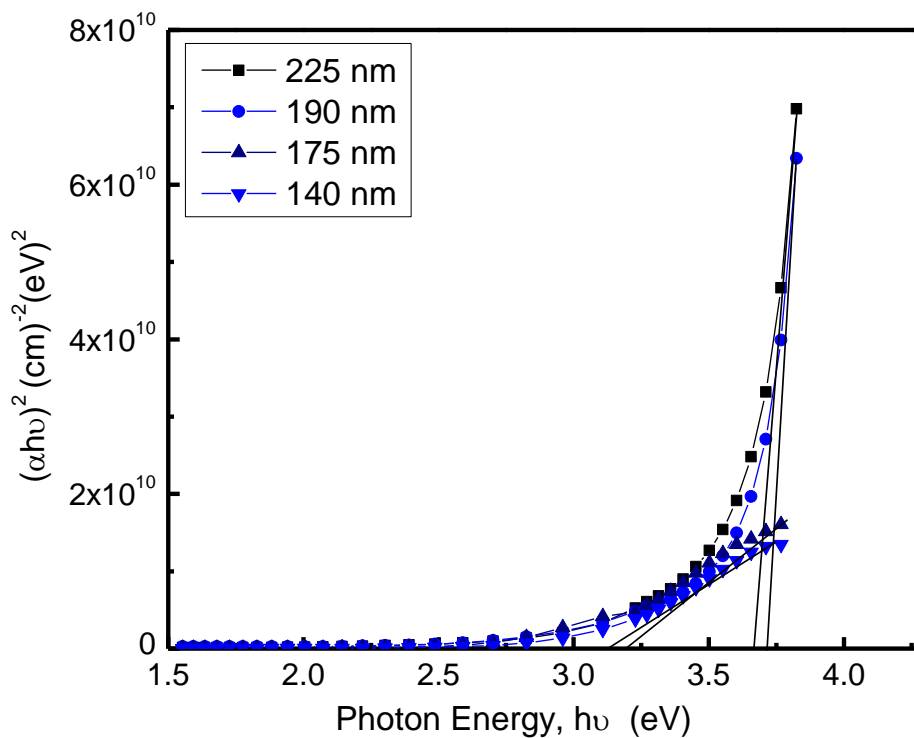

Fig. 4.8: $(\alpha h\nu)^2$ vs. $h\nu$ curves for PP(OMA-TMA) thin films of different thicknesses.

Table 4.5: Band gaps of PPOMA and PPTMA thin films

PPOMA thin films [4.4]			PPTMA thin films [4.10]	
Thickness d (nm)	E_{gd} (eV)	E_{gi} (eV)	Thickness d(nm)	E_{gi} (eV)
100	2.90	1.68	300	1.86
200	3.08	2.05	400	1.56
300	303	1.81	500	1.49

In Table- 4.4 it is seen that the values of E_{gd} and E_{gi} are found to be between 3.13 to 3.73 eV and 1.95 to 2.23 eV respectively for samples of different thicknesses. It is noticed that the values of E_g decreases with decreasing thickness of PP(OMA-TMA) thin films. Table 4.5 shows that the values of E_{gd} and E_{gi} of PP(OMA-TMA) are small increasing from PPOMA or PPTMA. Table 4.4 also shows that the values of E_{gd} are centered at 3.42 eV with a small variation. This is supported by the small variation of λ_{max} for different thickness of PP(OMA-TMA) thin films. This means that the thickness affects E_g due to the structural change in the composite thin films as observed in the modification/ shift of FTIR bands.

4.6   DC Electrical Properties

4.6.1   Current density-voltage characteristics

Current density-voltage (J-V) characteristics of PP(OMA-TMA) thin films of different thicknesses at the temperature of 298, 323, 348, 373 and 398 K were measured in the voltage region from 0.1 to 55 V. The observed J-V characteristics of the composite thin films are presented in Figs. 4.9 to 4.11. It is seen that J-V curves follow a power law, *Eq^n* 2.9 (Chapter II), with different slopes in the higher and lower voltage regions. The values of the slope are recorded in Table 4.6. In the lower voltage regions the values of the slope (n) lie between $0.51 \leq n \leq 1.3$ and in the higher voltage region the slopes is found between $2.43 \leq n \leq 4.95$ for all samples corresponding to ohmic and non ohmic regions respectively.

n values obtained from the voltage dependence of current density at the higher voltage region predict that the transport of carriers may be due to SCLC, Schottky or PF mechanism in PP(OMA-TMA) thin films [4.8, 4.9]. The conduction mechanism in PP(OMA-TMA) thin films can be identified from the dependence of J on film thickness, d for a series of different samples at constant voltage non-ohmic region the

J-d curve is presented in Fig. 4.14. The linear slope derived from these data has a value around -8.52. The value indicated that in the non-ohmic region the value of the slope satisfies the condition for SCLC mechanism (Chapter II, Sub. Sec. 2.9.3). So the type of conduction mechanism in PP(OMA-TMA) is SCLC.

Table 4.6: Slopes in the two voltage regions for different thicknesses and different temperatures

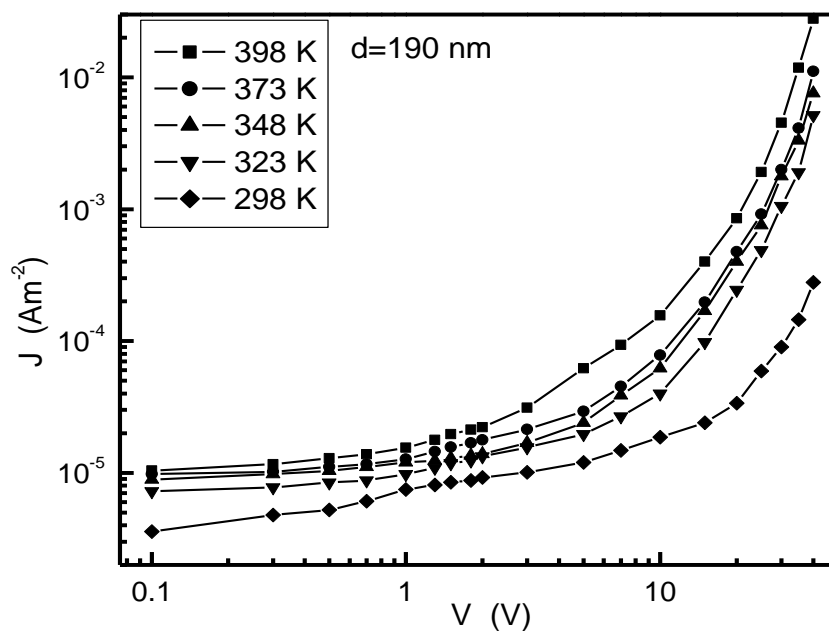| Thickness of PP(OMA-TMA) thin films d (nm)	Measurement temperature T (K)	Value of slopes, n	
		Low Voltage region (ohmic)	High Voltage region (Non ohmic)
190	298	0.57	3.02
	323	0.76	3.88
	348	1.07	4.13
	373	1.04	4.14
	398	1.30	4.75
165	298	0.55	3.27
	323	0.51	3.56
	348	0.52	3.97
	373	0.52	3.98
	398	1.09	3.91
110	298	1.01	2.98
	323	1.11	3.59
	348	0.91	3.78
	373	0.95	2.43
	398	0.91	2.59
75	298	0.58	4.95
	323	0.91	4.80
	348	0.90	4.15
	373	1.09	3.20
	398	1.25	3.21

Fig. 4.9: Plots of current density against applied voltage at different temperature for PP(OMA-TMA) thin film.
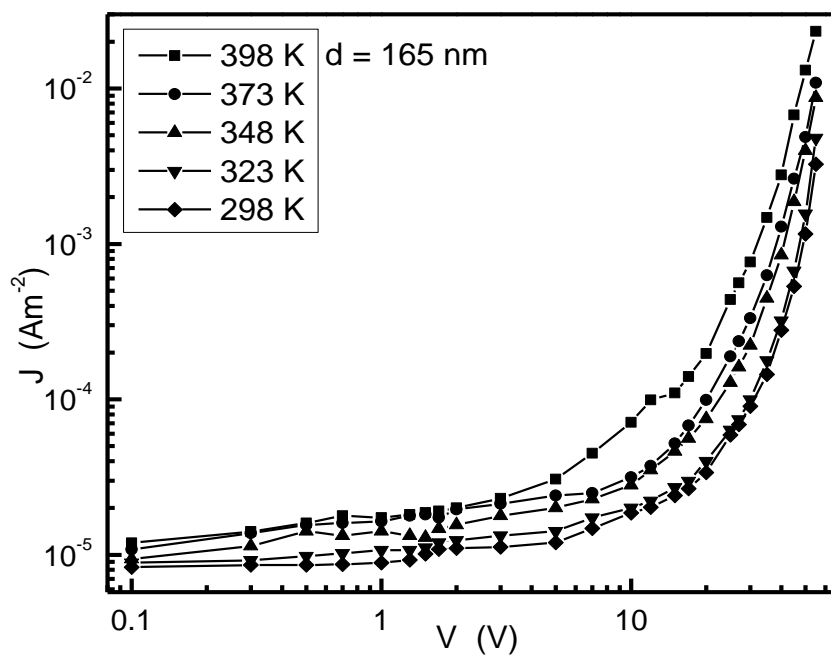

Fig. 4.10: Plots of current density against applied voltage at different temperature for PP(OMA-TMA) thin film.
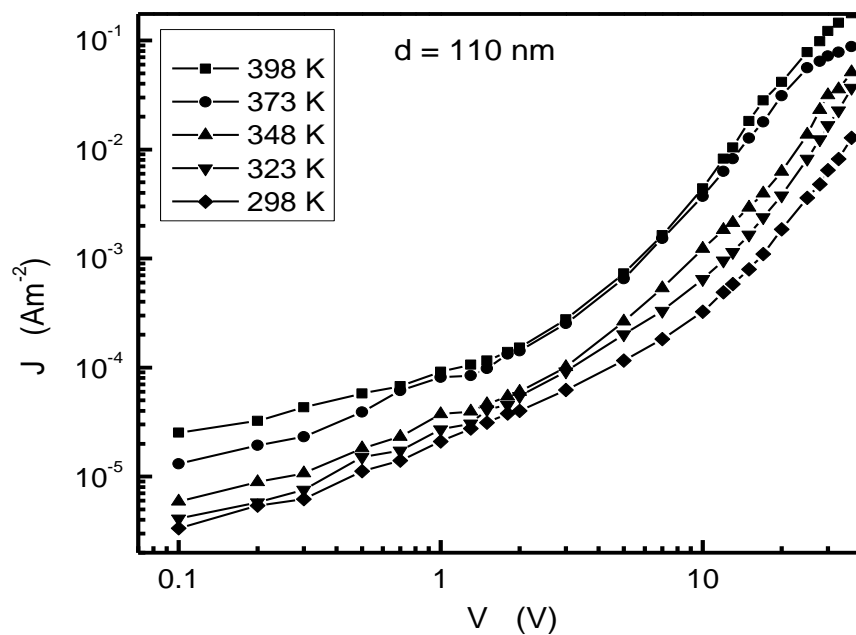
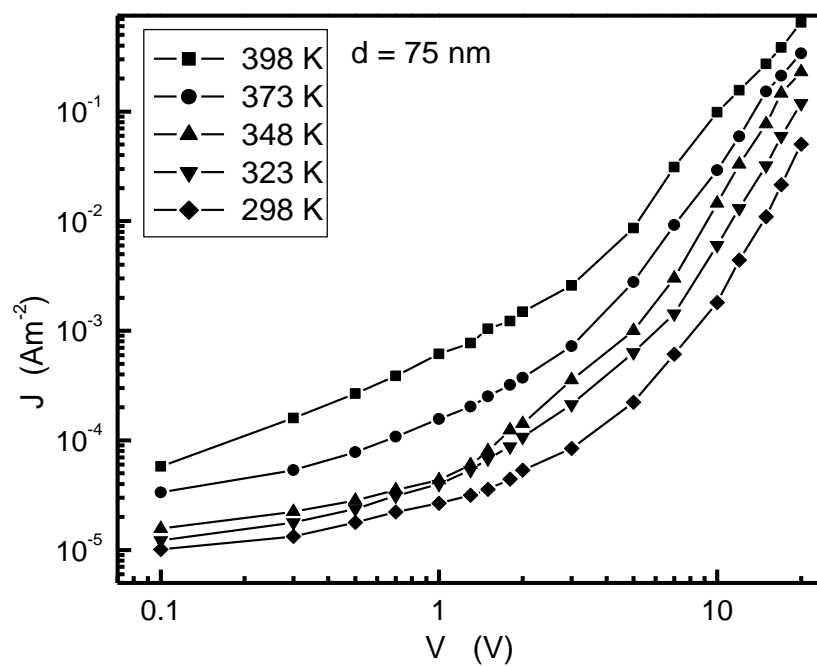Fig. 4.11: Plots of current density against applied voltage at different temperature for PP(OMA-TMA) thin film

Fig. 4.12: Plots of current density against applied voltage at different temperature for PP(OMA-TMA) thin film
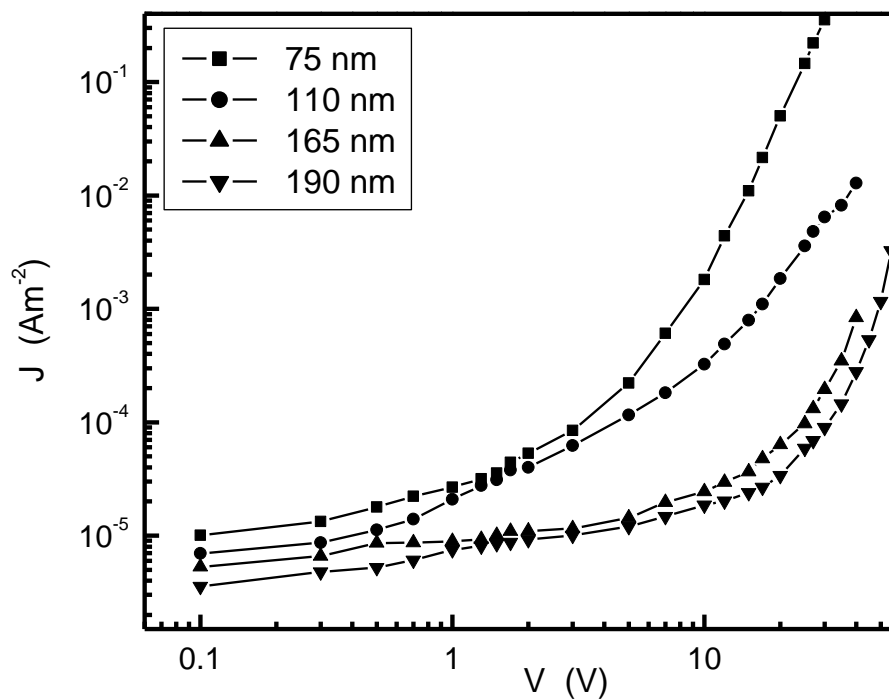
Fig. 4.13: Room temperature *J-V* curve of four samples of different thickness.
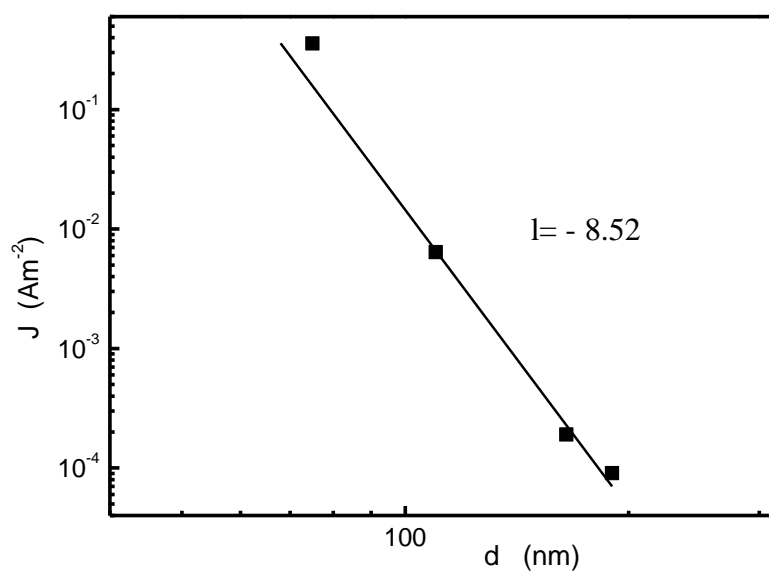

Fig. 4.14: Plots of room temperature current density against thicknesses of the different PP(OMA-TMA) thin films in the non-ohmic region (V=30 V).
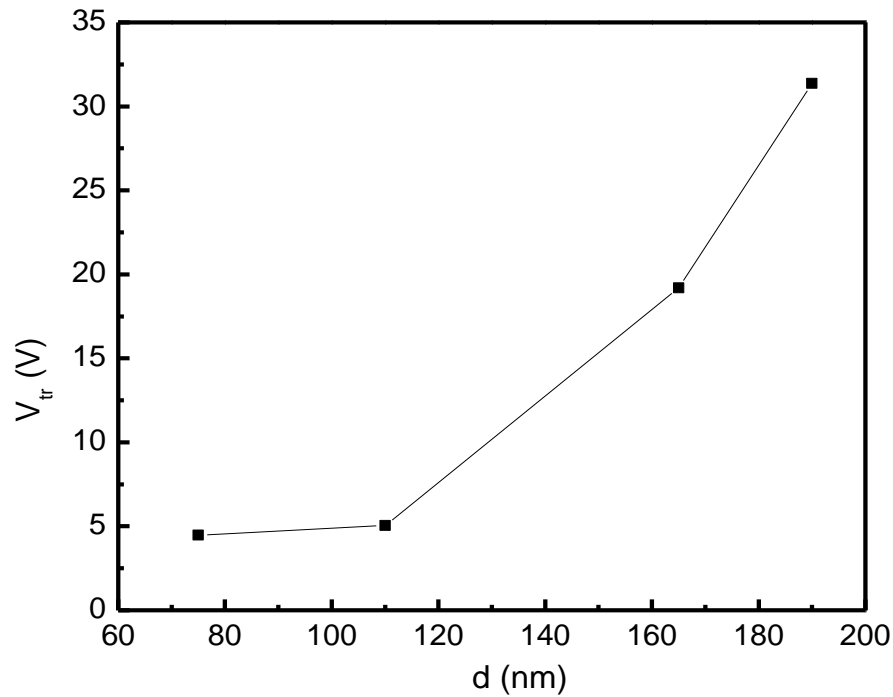
Fig. 4.15: Plots of d (nm) against V_{tr} (V) of PP(OMA-TMA) thin films

4.6.2 Temperature dependence of current density

The temperature dependence of the current density, *J*, can be expressed by the well-known Arrhenius law

$$J = J_0 \, exp\left(-\tfrac{\Delta E}{kT} \right)$$

$$(4.3)$$

where J_0 is a constant, ΔE is the thermal activation energy of electrical conduction and *k* is the Boltzmann constant. Fig. 4.16 to Fig 4.19 shows the dependence of *J* on inverse absolute temperature, *1/T*, for PP(OMA-TMA) thin films of different thicknesses. In these figures there are two curves, corresponding to the temperature dependence in the ohmic (V= 8 V) and in the SCLC regions (V= 30 V) respectively. It is observed that the current density increases slowly for temperatures <353 K and above 353 K *J* increases rapidly with temperature. This increase in *J* with temperature may be due to the increased movement of the adventitious ions and/or electrons. It is seen that both the curves can be characterized by two different slopes in the low and high temperature regions. The curves have varying slope at low temperatures but become almost linear in the high temperature region, corresponding to well-defined activation energy. The activation energies associated with two temperature regions were calculated from the

slopes of J vs $\dfrac{1}{T}$ plots for PP(OMA-TMA) of thicknesses 190, 165, 110 and 75 nm

and are presented in Table 4.7. For applied voltage of 8 V, at low temperature region the activation energies are found to be around   0.15 ± 0.05 eV and at higher temperature region it is 0.40 ±0.10 eV. Whereas, the low and high temperature region activation energies are found to be 0.19 ± 0.05 eV and 0.72 ± 0.22 eV for an applied voltage of 30 V. The low activation energies in the low temperature region indicate that the thermally activated hopping conduction is operative in this material. This change in ΔE from lower to higher values may be attributed to a transition from a hopping regime to a regime dominated by distinct energy levels [4.9]. Table 4.7 and Table 4.8 also show that the values of activation energy for PP(OMA-TMA) composite thin films are decreasing from PPTMA thin films.

Table 4.7: The values of activation energy ΔE (eV) for PP(OMA-TMA) thin films of different thicknesses.

Thickness d (nm)	Activation energy, ΔE (eV)			
	8 V		30 V	
	Temperature		Temperature	
	Low	High	Low	High
190	0.10	0.31	0.17	0.50
165	0.21	0.28	0.24	0.82
110	0.10	0.52	0.18	0.94
75	0.13	0.42	0.13	0.50

Table 4.8. Values of activation energy (eV), for various PPTMA thin films

Thickness d (nm)	Activation energy, ΔE (eV) [4.8]			
	2 V		10 V	
	Temperature		Temperature	
	Low	High	Low	High
300	0.20	0.89	0.18	0.90
350	0.18	0.76	0.22	0.79
400	0.17	0.72	0.18	0.82
500	0.19	0.88	0.18	0.88

Fig. 4.16: Variation of current density against inverse absolute temperature for PP(OMA-TMA) thin film in ohmic and non-ohmic regions.

Fig. 4.17: Variation of current density against inverse absolute temperature for PP(OMA-TMA) thin film in ohmic and non-ohmic regions.
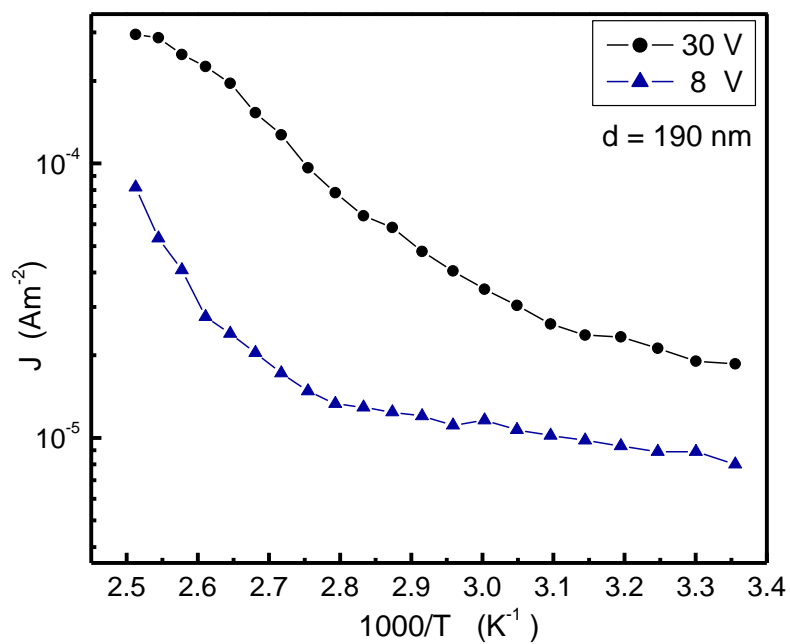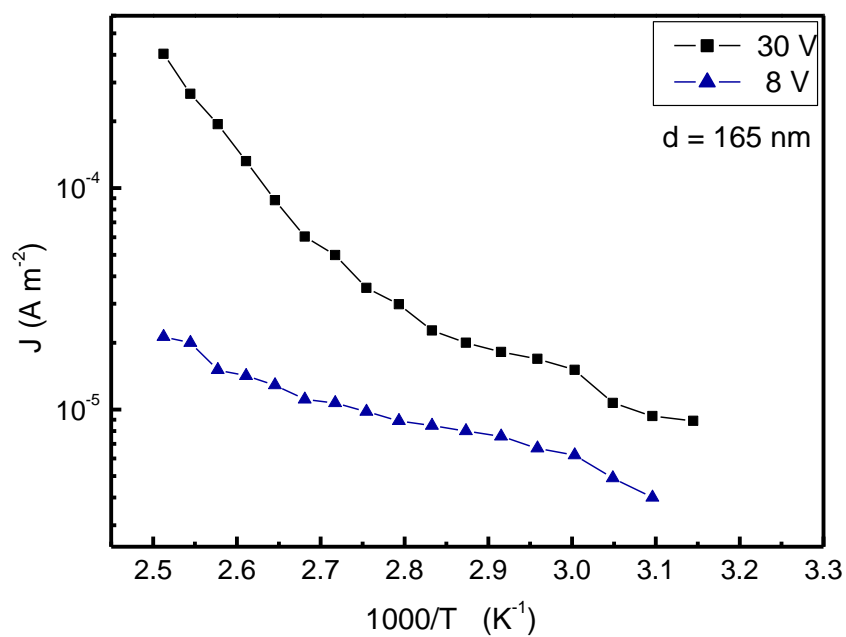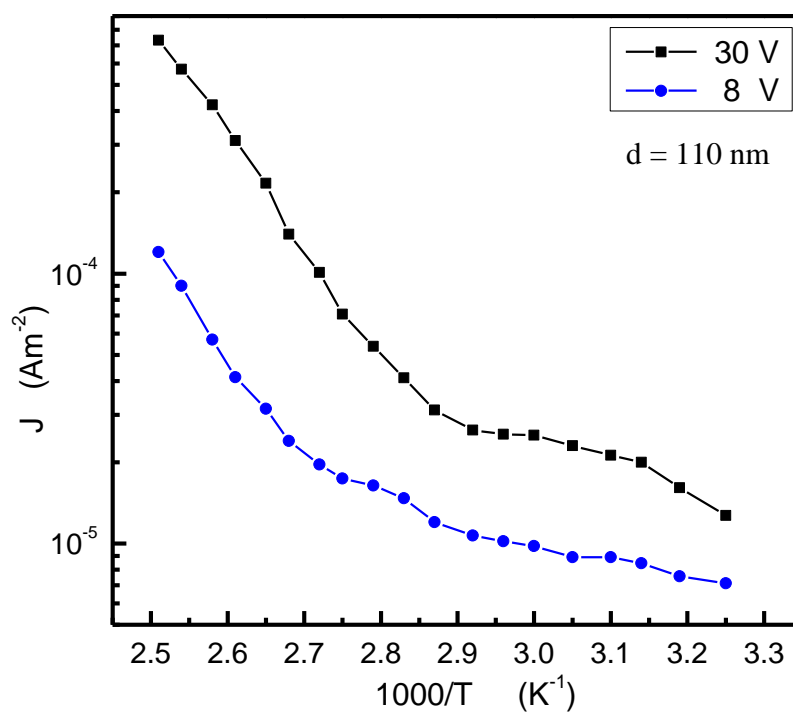
Fig. 4.18: Variation of current density against inverse absolute temperature for PP(OMA-TMA) thin film in ohmic and non-ohmic regions
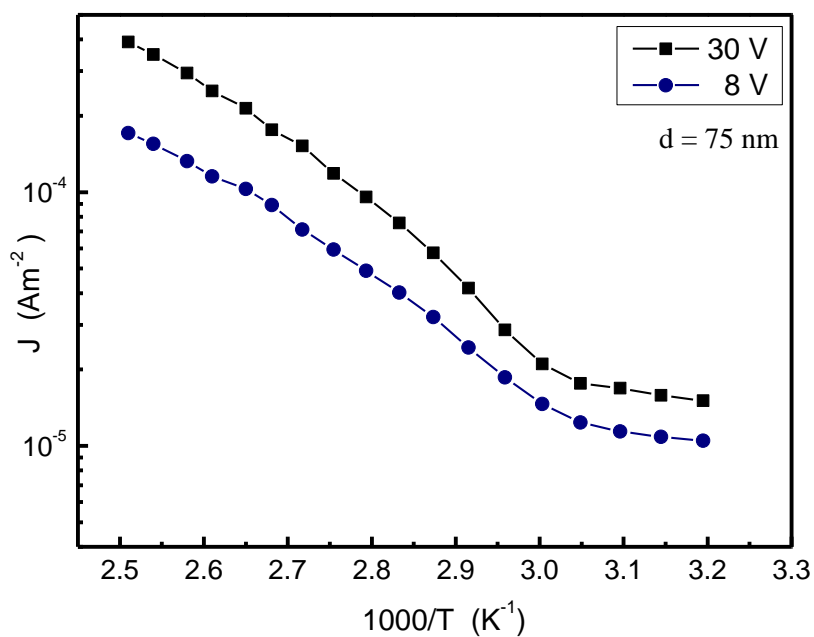

Fig. 4.19: Variation of current density against inverse absolute temperature for PP(OMA-TMA) thin film in ohmic and non-ohmic regions

Reference:

[4.1]   Inagaki, N., "Plasma Surface Modification and Plasma Polymerization", Tehnomic Publishing Co. Inc. UA, (1996).

[4.2]   Morosoff N in: R. d'Agostino (Ed), "Plasma Deposition, Treatment, and Etching of Polymers", Academic Press, San Diego, CA, (1990).

[4.3]   Chowdhury, F-U-Z, Ph. D. Thesis " Preparation and Characterization of Plasma – Polymerized Diphenyl Thin Films", Bangladesh University of Engineering and Technology (BUET), Dhaka, (2000).

[4.4]   Rahman, Mohammad Jellur and Bhuiyan, A.H.,"Structural and optical properties of plasma polymerized o-methoxyaniline thin films", Thin Solid Films, 534, 132–136, (2013).

[4.5]   Akther, H. and Bhuiyan, A. H., "Infrared and ultraviolet-visible spectroscopic investigation of plasma polymerized N,N,3,5–tetrametlylaniline thin films", Thin Solid Films, 474, 14 – 18, (2005).

[4.6]   Robert T. Conley., "Infrared spectroscopy", Allyn and Bacon Inc., Boston, (1975).

[4.7]   Davis, E. A. and Mott, N. F., "Conduction in non-crystalline system, Optical absorption and photoconductivity in amorphous semiconductors", Philos. Mag. **22,** 903-922, (1970).

[4.8]   Akther H. and Bhuiyan A. H. 'Space charge limited conduction in plasma polymerized N, N, 3, 5 tetramethylaniline thin films' New J. Phys. 7, 173, (2005).

[4.9]   R. D. Gould, 'The interpretation of space-charge-limited currents in semiconductors and insulators', J. Appl. Phys. 53 (1982) 3353.

[1.10] Akther, H. and Bhuiyan, A. H., "Electrical and optical properties of plasma polymerized N, N, 3, 5 tetramethylamiline thin films", New J. Phys. 7**,** 173-176, (2005).

CHAPTER V

CONCLUSIONS

5.1   Conclusions

Plasma polymerization method was used to get PP(OMA-TMA) composite thin films of different thickness under glow discharge plasma using a capacitively coupled reactor. The structural and thermal analyses have been performed on the deposited PP(OMA-TMA) composite thin films. The thickness dependence of the optical properties of the PP(OMA-TMA) composite thin films were studied in the UV-Vis region of the electromagnetic spectrum. DC *J-V* characteristics of the PP(OMA-TMA) thin films of different thicknesses were studied at various temperatures. All these results are discussed in this thesis. The following conclusions can be drawn from these results and discussion.

The PP(OMA-TMA) thin films showed flawless, pinhole free, homogeneous and smooth surface having highest percentage of carbon and good percentage of nitrogen which is in PP(OMA-TMA) grown from mixed monomers. The percentage of oxygen in the polymer is slight higher due to the incorporation of oxygen from atmosphere and/or plasma reactor.

The chemical nature of PP(OMA-TMA) is observed to be somewhat different from those of the monomers, OMA and TMA, as found by FTIR spectroscopy. DTA and TGA traces showed that PP(OMA-TMA) was stable up to about 575 K. Above 575 K there is a gradual fall of DTA, may be a cause of thermal breakdown of PP(OMA-TMA) structure.

UV-Vis spectral behavior of PP(OMA-TMA) thin films showed that the absorbance increases with the increase in thickness. As the thickness of the films increases electronic transition occurs from the more depth of the samples which need more energy. It is found that the peak wavelength shifts to lower wavelength for composite thin films with increase in thickness. The dependence of α on the hν indicates that the absorption edge starts increasing around 2.25 eV and there is an exponential rise of α above 2.80 eV. The E_{gd} and E_{gi} of the studied PP(OMA-TMA) composite thin films are found in the range of 1.95 to 2.23 eV and 3.13 to 3.73 eV, respectively.

It is observed in the J-V characteristics of PP(OMA-TMA) composite thin films that J increases nonlinearly with the applied voltage having ohmic nature in the low and non-ohmic nature in the high voltage regions. The slope of the J-d plot in the non-ohmic region ascertains that the type of carrier conduction in PP(OMA-TMA) composite thin films is SCLC. Activation energies are found to be around 0.15 ± 0.05 eV at the low temperature region and at higher temperature region it is 0.40 ± 0.10 eV in the ohmic region. Whereas,

the low and high temperature region activation energies are found to be 0.19 ± 0.05 eV and 0.72 ± 0.22 eV in the non-ohmic region. The temperature dependence of J suggests that the electrical conduction in PP(OMA-TMA) composite thin films may be due the thermally activated charge carriers in the high temperature region and hopping in the low temperature region.

From the above conclusions it can be inferred that PP(OMA-TMA) composite thin films have different electrical and optical behaviors compared to the thin films of individual monomers.

5.2   Suggestions for Further Work

In the present work the thermal, optical and ac electrical behavior of PP(OMA-TMA) thin films are investigated. More investigations are needed to explain different properties elaborately, which will help finding appropriate application of this composite material. The following investigations may be carried out for further study.

The AC electrical properties can be carried out for the PP(OMA-TMA) thin films in different conditions. The dielectric constant, loss factor and the ac conductivity may be measured after heat treatment or aging to find the dielectric applications of the material. The engrossing character of multi-layer composite thin films played a vital role in determining the physical characteristics of the composite thin films. The probable in homogeneities, disorderness and irregularities of the interface may be affected the optical band gaps as well as the electrical conductivity of the films.

DTA, TGA and DSC at different heating rate can be performed for thermal analyses which will be help to determine the reaction kinetics in the PP(OMA-TMA) thin films.